





## Article

# Analyzing and Modeling the Spatial-Temporal Changes and the Impact of GLOTI Index on Precipitation in the Marmara Region of Türkiye

Mehdi Aalijahan <sup>1</sup>, Atilla Karataş <sup>1</sup>, Anthony R. Lupo <sup>2</sup>, Bahtiyar Efe <sup>3</sup> and Azra Khosravichenar <sup>4,5,\*</sup>

<sup>1</sup> Faculty of Human and Social Sciences, Geography Department, Marmara University, Istanbul 34722, Türkiye

<sup>2</sup> School of Natural Resources, University of Missouri, Columbia, MO 65202, USA

<sup>3</sup> Department of Meteorological Engineering, University of Samsun, 19 Mayıs, Samsun 55420, Türkiye

<sup>4</sup> Institute of Geography, Leipzig University, 04103 Leipzig, Germany

<sup>5</sup> Institute of Geography, Technische Universität Dresden, 01069 Dresden, Germany

\* Correspondence: azra.khosravichenar.2@uni-leipzig.de

**Abstract:** Precipitation is a particularly important part of the Earth's hydrological cycle and, therefore, is a necessary variable for maintaining natural balance. This study investigated past, present, and future changes in precipitation in the Marmara region, and examined the effects of global warming on this variable. The study period was from 1960 to 2020, and the climate data of 15 synoptic stations in the Marmara region were used for this purpose. To achieve the objectives of the study, linear and 6th order polynomial regression, ombrothermic and hythergraph diagrams, geostatistical models, Mann-Kendall test, Pearson correlation, standard Z-scores, and multi-layer perceptron artificial neural network models (MLP-ANN) were used to model and predict precipitation. The results of the linear regression analysis showed that of the 15 stations, 6 stations had an increasing trend, 6 stations had a trendless pattern, and 3 stations had a decreasing trend. In terms of periodic analysis, the main downward trend started in 1964 and continued until 1992, while the main periodic upward trend started in 1992 and continued until 2016. The synoptic stations in the Marmara region showed a lack of precipitation over six to seven months of the year, and the precipitation changes in the region were stronger than the temperature changes. In addition, the highest precipitation was observed on the southeast coast of the Black Sea, and the lowest precipitation was observed in the eastern parts of the region. Moreover, except for the Bilecik and Kocaeli stations, the changes in the long-term trend of precipitation at the other stations were significant. Among the 15 stations, only the Kocaeli and Saryyer stations showed a positive correlation with global temperature during the annual period. In addition, the developed ANN model was accurate in simulating and predicting precipitation and showed an upward trend over the next seven years.

**Keywords:** precipitation modeling; machine learning; MLP-ANN model; trend analysis; Mann-Kendall test; GLOTI index; global warming effect; Marmara region



**Citation:** Aalijahan, M.; Karataş, A.; Lupo, A.R.; Efe, B.; Khosravichenar, A. Analyzing and Modeling the Spatial-Temporal Changes and the Impact of GLOTI Index on Precipitation in the Marmara Region of Türkiye. *Atmosphere* **2023**, *14*, 489. <https://doi.org/10.3390/atmos14030489>

Academic Editor: Corene Matyas

Received: 28 January 2023

Revised: 22 February 2023

Accepted: 25 February 2023

Published: 1 March 2023



**Copyright:** © 2023 by the authors. Licensee MDPI, Basel, Switzerland. This article is an open access article distributed under the terms and conditions of the Creative Commons Attribution (CC BY) license (<https://creativecommons.org/licenses/by/4.0/>).

## 1. Introduction

Precipitation is one of the most important inputs for applications in hydrology, climate change, and ecological research since it exhibits large variability at spatial and temporal scales, with spatiotemporal heterogeneity having a significant impact on the hydrological cycle and land surface processes [1–7]. Over the past decade, there has been an increasing interest in studying precipitation regimes, both globally and regionally, in the context of global warming. Most researchers believe that the 0.74 °C–0.85 °C increase in global average air temperature over the last hundred years (1880–2012) [8,9] has caused an increase in the amount of water vapor in the atmosphere and changes in the hydrologic cycle and atmospheric circulation. It has also been emphasized that the global increase in precipitation frequency and intensity, especially in extreme precipitation, causes flooding, landslides,

and loss of life [10–17]. Some studies have shown an increase in the intensity and frequency of potentially hazardous precipitation in the mid-latitudes of the Northern Hemisphere, especially north of 35°N latitude [11,18,19]. The average global precipitation is likely to increase owing to increases in the atmospheric moisture storage capacity associated with global warming [20]. However, future precipitation changes were not uniform. By the end of the 21st century, the average annual precipitation is expected to increase at high latitudes, the equatorial Pacific, and many humid mid-latitude regions, whereas it is expected to decrease in many dry mid-latitudes and subtropical regions. Observations have indicated an increase in average precipitation over land areas in the mid-latitudes of the Northern Hemisphere since 1951 [21].

The Mediterranean basin is located in the transition zone between the temperate and rainy climate of southern Europe and the arid climate of northern Africa and is potentially vulnerable to climate change [22]. In recent decades, winter precipitation in the Mediterranean region has shown a general downward trend in recent decades [23–26]. The eastern Mediterranean region has been prone to climatic conditions of drought since the mid-20th century [27–30]. In Türkiye, there are spatial differences in precipitation between the southern coast and the northern and western coastal regions [31,32] and between coastal and mountainous regions [33].

One of the coastal regions of Türkiye is the Marmara region which accounts for 40% of Türkiye's population, production, trade, and cultivation, and is considered the country's most important economic resource.

Due to excessive population growth in the region and increased migration to the region, the supply of water for various industrial, agricultural, and potable purposes will be one of the major challenges for the responsible organizations. Therefore, analyzing the precipitation trend and its long-term changes over 61 years, studying the impact of global warming on precipitation in the region, and predicting the trend of precipitation changes over the next seven years can provide comprehensive and accurate information and data to researchers and decision-makers. Therefore, the main objectives of this study are the following:

- To study the general situation of precipitation in the Marmara region during the last 61 years.
- To analyze the changes and variations of precipitation trends in the Marmara region during the last 61 years.
- Investigation of the annual and seasonal spatial distribution of precipitation in the Marmara region.
- Analysis of the impact of climate change and global warming on precipitation in the Marmara region.
- Modeling and prediction of precipitation in the Marmara region for the next 7 years.

## 2. Data and Methods

### 2.1. Study Area

The Marmara region (Figure 1), with a total area of 67,306 km<sup>2</sup>, is located in the most industrialized and populated region of Türkiye [34] which is covered by low-lying valleys and plateaus. Its climate is a mixture of Mediterranean and humid subtropical climate on the Aegean and southern Marmara Sea coasts, oceanic climate on the Black Sea coasts, and humid continental climate in the interior of Thrace and Anatolia with hot and moderately dry summers and cold, rainy, and sometimes snowy winters. The average annual temperature in Marmara was 14 °C; the average temperature in January, the coldest month, was 4.9 °C, and the average temperature in July, the warmest month, was 23.7 °C. Coastal climate provides relatively mild temperatures. The average annual relative humidity in the area was 73%. The average annual precipitation in the region is 690 mm, with strong spatial variations: 800 mm in the eastern part of the region and less than 600 mm in the central and western parts [35,36].

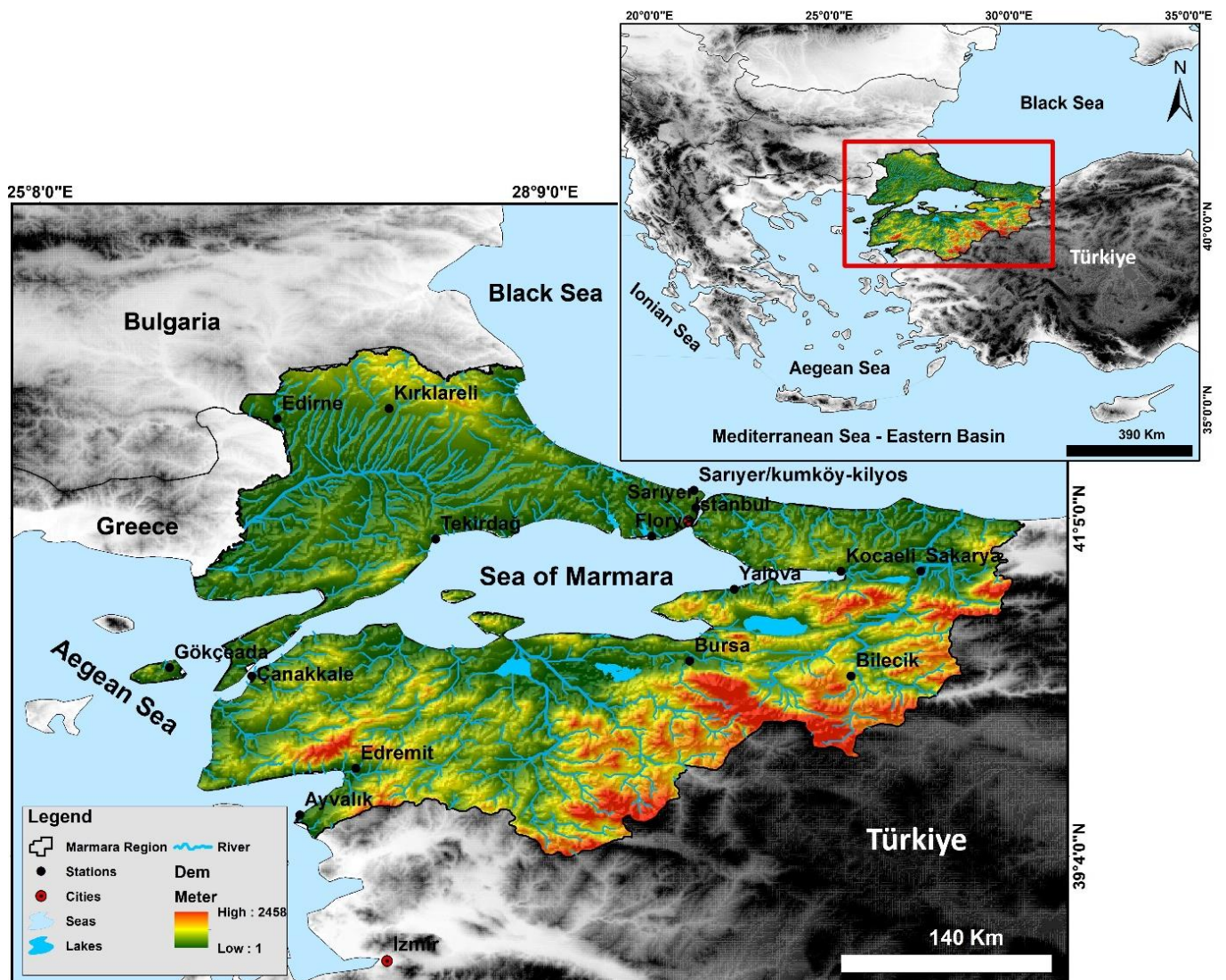


Figure 1. The location of the study area and distribution of the synoptic stations.

## 2.2. Data

Two data categories were used in this study. The first category includes precipitation, temperature, wind, humidity, barometric pressure, and sunshine data related to the synoptic stations. For this study, 15 synoptic stations (Table 1) in the study area with long-term records starting from 1960 to 2020 were used. The second category of data is the index of global land-ocean temperature anomalies (GLOTI index), known as global warming data, obtained from the NOAA organization website (<https://data.giss.nasa.gov/gistemp/> (accessed on 24 February 2023)).

## 2.3. Methods

The general procedure of the study is as follows. First, statistical analysis was conducted on the precipitation data in the Marmara region. The situation, trends, changes, and variations in precipitation in the region were then studied. To understand the spatial distribution of precipitation in the region, the amount of precipitation was interpolated using a geostatistical analysis model, the radial basic function (RBF) method, in the GIS platform. A linear regression model and 6th-order polynomial regression were used to analyze the trends of precipitation and its changes and variations. Furthermore, ombrothermic and hythergraph diagrams were used to understand the precipitation situation in the region during the year [37,38]. In addition, the non-parametric Mann-Kendall test was used to

analyze and identify the trend changes in the precipitation data. To understand the impact of GLOTI index on precipitation in the Marmara region, both datasets were evaluated using the Pearson correlation and standard Z-scores. Finally, for modeling, simulation, and prediction of precipitation over the next seven years, first, the predictability of the precipitation variable was evaluated by the Hurst exponent using the Rescale Range (R/S) method, and then the precipitation variable was predicted using the machine learning and Multilayer Perceptron-Artificial Neural Network (MLP-ANN) method with the Broyden–Fletcher–Goldfarb–Shanno (BFGS) algorithm after normalization of precipitation data. In order to validate the performance of the developed MLP-ANN model, the R2 method was used. The main models used in the study are described in detail below and the flowchart of the study is shown in Figure 2.

**Table 1.** The specifications of the synoptic stations in the Marmara region.

Row	Station No	Station	Altitude (m)	Latitude (Degree)	Longitude (Degree)
1	17,175	Ayvalık	4	39.3113	26.6861
2	17,120	Bilecik	539	40.1414	29.9772
3	17,116	Bursa	100	40.2308	29.0133
4	17,112	Çanakkale	6	40.141	26.3993
5	17,050	Edirne	51	41.6767	26.5508
6	17,145	Edremit	21	39.5895	27.0192
7	17,636	Florya	37	40.9758	28.7865
8	17,110	Gökçeada	79	40.191	25.9075
9	17,052	Kırklareli	232	41.7382	27.2178
10	17,066	Kocaeli	74	40.7663	29.9173
11	17,059	Sarıyer/Kumköy-Kilyos	38	41.2505	29.0384
12	17,069	Sakarya	30	40.7676	30.3934
13	17,061	Sarıyer	59	41.1464	29.0502
14	17,056	Tekirdağ	4	40.9585	27.4965
15	17,119	Yalova	4	40.6589	29.2796

#### 2.4. Nonparametric Testing

Nonparametric statistics are generally much less affected by the presence of outliers and other forms of nonnormality [39] and provide a measure of monotonic linear dependence [40,41]. The most commonly used nonparametric test for determining trends in hydrologic, meteorological, environmental, and climate variables is the Mann-Kendall test (MK) [42,43]. The significant trend determined by the Mann-Kendall test (MK) can be supplemented with Sen's slope estimate to determine the magnitude of the trend. The non-parametric Mann-Kendall test and Sen's slope estimator have been applied to estimate trends in meteorological time series [44,45].

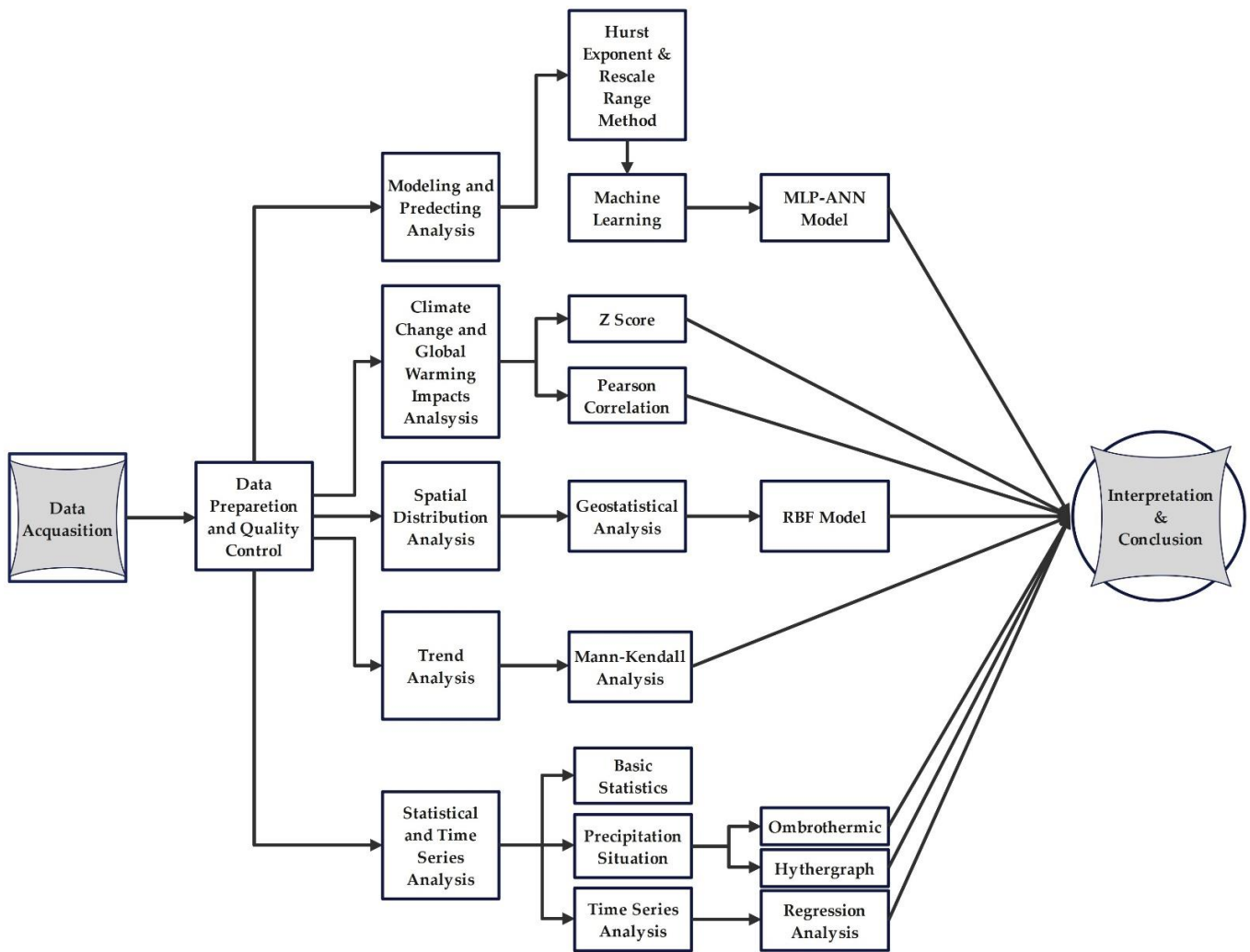


Figure 2. The flowchart of the study.

2.5. Mann-Kendall Test-Detection of Mutations

The Mann-Kendall test can also be used to detect sudden changes in climate and hydrological data [46–50]. For an assumed data series  $K (k_1, k_2, \dots, k_n)$   $n$  is the length of the data series. First, the cumulative statistic parameter  $S_k$ , being the cumulative number of values at time  $i$  that are greater than at time  $j$ , is calculated as follows:

$$S_k = \sum_{i=1}^k r_i \quad k = 2, 3, \dots, n, \tag{1}$$

$$r_i = \begin{cases} 1 & k_i > k_j \\ 0 & k_i \leq k_j \end{cases} \quad j = 1, 2, \dots, i - 1, \tag{2}$$

Subsequently, assuming random independence of the time series, the statistic parameter  $U'I$  can be defined as follows:

$$U'I = \frac{S_k - E(S_k)}{\sqrt{Var(S_k)}} \quad k = 1, 2, \dots, n, \tag{3}$$

$U'I = 0$ , and  $E(S_k)$  and  $Var(S_k)$  represent the expected value and variance of the cumulative value  $S_k$ , respectively, which are obtained as follows:

$$E(S_k) = \frac{k(k - 1)}{4}, \tag{4}$$

$$Var(S_k) = \frac{k(k-1)(2k-5)}{72}, \tag{5}$$

U'I is a standard normal distribution, i.e., a statistical sequence computed from the sequence of time series X. At a significant level  $\alpha$ , a condition of  $|U'I| > U_\alpha$  indicates an apparent trend change within the time series. Using the inverse time series, we calculated U'I again applying the calculation procedure described above, where  $UI = -U'I$  and  $k = n, n-1, \dots, 1$  [51]. Where the curves of UI and U'I intersect, the starting point of the trend and changes are approximated. If the curves intersect within the range of  $(\pm 1.96)$ , it is the beginning of a sudden change. However, if they intersect outside the critical range, it indicates the presence of a trend in the time series. Also, when multiple breakpoints occur near each other, the last one will be considered the breakpoint [52]. Before performing this technique, the run test was performed on the data to ensure that the data was not digressive. All of the Mann-Kendall analyses were performed using MATLAB software.

### 2.6. MLP-ANN Model

The MLP-ANN model is the most extensively used type of ANN's approach for modeling hydrological and climatological data [53]. The MLP network is a feedforward ANN consisting of three layers, input layers, hidden layers, and output layers with a set of neurons and activation function as shown in Figure 3. Each of the neurons in the input is connected to all of the neurons of the intermediary, and it is connected to all neurons in the output layer [54–58]. A feedforward ANN is a basic type of ANN that is capable of approximating both continuous and integrable functions [59]. The mathematical structure of the feed forward multilayer perceptron with one output node can be represented by the following equation [60,61]:

$$y_1 = S_1 \left( \sum_{j=1}^{N_j} w_j S_2 \left( \sum_{i=1}^{N_i} w_i x_i \right) \right), \tag{6}$$

where  $y_1$  is the output ( $[0, 1]$ ) of the network,  $x_i$  is the input array (Figure 3),  $w_i$  the connection weights between the data node and the hidden layer,  $w_j$  is the connection weights from the hidden layer to the output layer,  $S_1$  is the activation function from the Input layer to the hidden layer,  $S_2$  is the activation function from the hidden layer to the output layer.

The MLP networks can approximate universal functions and give the solution of different tasks such as information processing, recognition of standards, weather forecasts, image processing, activity forecasts, and others [62].

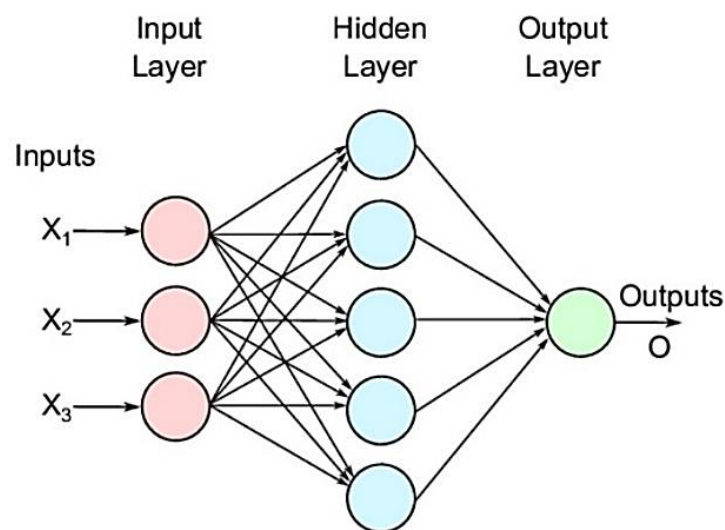


Figure 3. An example of MLP network architecture with one hidden layer [63].

The neurons compute a single output from multiple real-valued inputs  $\{x(t)\}$  by forming a linear combination between inputs weights and then subjected the output to some nonlinear function according to Ref. [64] given as:

$$y(t) = v_o + \sum_{i=1}^N v_i \Psi \left( b_i + \sum_{j=1}^n w_{ji} x_j(t) \right), \tag{7}$$

where  $b_i$  is the bias in the hidden layer,  $w_{ij}$  is the weight of the connection between neuron in the hidden layer and neuron in the input layer,  $v_i$  is the weight of the connection between neuron in the hidden layer and neuron in the output layer,  $N$  is the number of neurons in the hidden layer,  $\Psi$  is the transfer function, and  $y(t)$  is the single output of MLP network. The expression in the parenthesis is defined as the perceptron type neurons according to Ref. [65]. MLP is usually trained using the back-error propagation algorithm to minimize errors in the same direction until the steady state is reached [66]. A logistic function was used as the transfer function in the hidden layer in this study given as:

$$f(x) = \frac{1}{1 + e^{-x}}, \tag{8}$$

where  $x$  is the input variable. Thus, in addition to logistic function as a transfer function, the output of MLP-ANN can be further improved during the training processes by adjusting the weights in the hidden layer using appropriate training algorithms. In this study, several training algorithms are tested out and between them the Broyden–Fletcher–Goldfarb–Shanno (BFGS) algorithm was chosen as the best algorithm due to its good training, validation, and test performance and lower errors.

### 2.7. Broyden–Fletcher–Goldfarb–Shanno Algorithm (BFGS)

In numerical optimization, the Broyden–Fletcher–Goldfarb–Shanno (BFGS) algorithm is an iterative method for solving unconstrained nonlinear optimization problems [67,68]. BFGS algorithm was implemented by estimating the inverse odd Hessian function,  $H$  directly with a symmetric positive definite matrix  $P$  iteratively using the following steps [69]:

Step 1: The search direction  $d_k$  was set to be equal to  $-P_{k-1}g_k$  where  $-P_{k-1}$  and  $g_k$  are the approximation to inverse  $H_{k-1}$  and its gradient, respectively, at the  $k$ th iteration. The convergence tolerance was set to be a minimum value of order  $10^{-3}$ .

Step 2: The weights which yield the minimum error along  $d_k$  was found as:

$$w_{k+1} = w_k + \eta_o d_k, \tag{9}$$

$$\eta_o = \min(E(w_k + \eta d_k)), \tag{10}$$

Step 3: The new gradient  $g_{k+1}$  was computed and the approximation to  $P_k$  was updated using the new weight and gradient information given as:

$$s_k = w_{k+1} - w_k \text{ and } y_k = g_{k+1} - g_k, \tag{11}$$

$$U_k = \left( 1 + \frac{y_k^T P_k y_k}{s_k^T y_k} \right) \frac{s_k^T s_k}{s_k^T y_k}, \quad V_k = \frac{y_k^T P_k y_k + P_k y_k s_k}{s_k^T y_k}, \tag{12}$$

$$P_k = P_{k+1} + U_k + V_k, \tag{13}$$

The initial approximation to the inverse Hessian matrix ( $P_o$ ) is an identity matrix ( $I$ ) which corresponds to the steepest descent ( $d_k = -g_k$ ). Matrices  $U$ ,  $V$ , and  $P$  are symmetric and therefore lead to a reduction of weight errors to meet the convergence tolerance [70].

### 2.8. Normalization of Data

By considering the nature of sigmoid function adopted in ANN, the training data set values are normalized between 0 and 1 by Equation (14) and passed into the network. After

the completion of training, the output values are denormalized to provide the results in original domain.

$$NOR(P_i) = \frac{P_i - Min(P_i)}{Max(P_i) - Min(P_i)}, \tag{14}$$

where  $NOR(P_i)$  is the normalized value of  $P_i$ ,  $Min(P_i)$  is the series minimum value of  $P_i$  and  $Max(P_i)$  is the series maximum value of  $P_i$  [71,72].

2.9. Measuring the Performance of the Model

Performances of all networks are measured by coefficient of correlation,  $R^2$ , given by Equation (15) [73]:

$$R^2 = 1 - \frac{\sum_{i=1}^m (X_i - Y_i)^2}{\sum_{i=1}^m (\bar{Y} - Y_i)^2}, \tag{15}$$

where:

- $X_i$ : Is the predicted  $i$ th value
- $Y_i$ : Element is the actual  $i$ th value
- $\bar{Y}$ : Average of the all  $Y$  value

2.10. Hurst Exponent Computation with Using of Rescale Range (R/S) Analysis Method

The Hurst exponent measures the long-term memory spread of a data set [74,75]. Several techniques/methods are preferred by different researchers for estimating the Hurst exponent, of which the rescale range (R/S) analysis method is the most commonly used in the fields dealing with complex time series [76–80]. In the work of [81], the robustness of the R/S method compared to the fractional Gaussian noise model for estimating the Hurst exponent is demonstrated and recommended for use. Therefore, the R/S analysis method was used in this study. For non-stationary time series, R/S analysis may yield a Hurst exponent greater than 1 [82]. In this case, the detrended fluctuation analysis method may be considered. R/S analysis is a means of characterizing the time series, and its operation is summarized as follows. The first step is to decompose the time series into many shorter series. Hurst [83] proposed the following five general equations for R/S analysis, which can be used for any time series and are not limited to Brownian motion time series:

$$\left(\frac{R}{S}\right)_s = ks^H, \tag{16}$$

where  $k$  is a constant and  $s$  is the length of each of the shorter time series;  $1 \leq s \leq N$ ,  $N$  being the entire length of the time series.  $R$  is the range of the time series and  $S$  is the standard deviation.

The range of each size is calculated as [82]:

$$R = \max(z_1, z_2, z_3, \dots, z_s) - \min(z_1, z_2, z_3, \dots, z_s) \quad s = 1, 2, \dots, N, \tag{17}$$

$z_s$  is the cumulative series estimated as:

$$z_s = \sum_{i=1}^s y_i, \tag{18}$$

where  $s = 1, 2, \dots, N$ .  $y_s$  is the adjusted time series estimated by subtracting the sample mean from each of the shorter time series as:

$$y_s = x_s - \bar{x}, \tag{19}$$



where  $s = 1, 2, \dots, N$  and

$$\bar{x} = \frac{\sum_{i=1}^N x_i}{N}, \quad (20)$$

The Hurst exponent is estimated as the slope of the line plotted between  $(R/S)_s$  and  $s$  on a log–log scale.

### 3. Results

#### 3.1. Basic Statistics Analysis

Table 2 shows the annual statistics of the precipitation variables at the synoptic stations. According to the table, the lowest average precipitation falls at the Bilecik station at 462.10 mm and the highest average precipitation falls at the Sakarya station at 849.70 mm. Among the studied stations, Edremit and Gökçeada stations had the highest annual precipitation variation coefficient for 61 years with 25%, whereas Sakarya station had the lowest annual precipitation variation coefficient of 16%.

**Table 2.** Basic statistics of annual precipitation at the synoptic stations in the study area.

Station	Mean (mm)	Std. Deviation (mm)	Minimum (mm)	Maximum (mm)	Range (mm)	CV (%)
Ayvalık	652.70	140.90	304.60	992.30	687.70	0.22
Bilecik	462.10	79.20	320.40	668.70	348.30	0.17
Bursa	698.60	139.50	446.40	1328.20	881.80	0.20
Çanakkale	615.60	137.90	343.90	977.70	633.80	0.22
Edirne	601.70	129.00	387.00	958.60	571.60	0.21
Edremit	700.00	174.10	377.00	1220.30	843.30	0.25
Florya	643.80	122.60	420.10	969.10	549.00	0.19
Gökçeada	748.80	189.40	326.00	1185.10	859.10	0.25
Kırklareli	580.10	142.00	326.60	990.30	663.70	0.24
Kocaeli	814.10	140.60	579.30	1180.80	601.50	0.17
Kumköy-Kilyos	807.60	170.40	470.60	1231.20	760.60	0.21
Sakarya	849.70	139.30	600.70	1268.50	667.80	0.16
Sarıyer	834.40	162.30	574.20	1218.80	644.60	0.19
Tekirdağ	579.90	132.80	334.60	896.30	561.70	0.23
Yalova	745.80	154.00	472.40	1293.20	820.80	0.21

#### 3.2. Time Series Analysis and Precipitation Situation in the Region

The results of the long-term analysis of the time series trend of precipitation by linear regression at the stations in the study area showed that the precipitation at these stations followed three patterns: no trend, upward trend (Figure 4a), and downward trend (Figure 4b). At the synoptic stations in the Marmara region, no trend was observed in the long-term time series of the Ayvalık, Bursa, Edremit, Kırklareli, Tekirdağ, and Yalova stations. Bilecik, Edirne, Kocaeli, Kumköy-Kilyos, Sakarya, and Sarıyer stations were among the stations with a long-term upward trend, whereas Çanakkale, Florya, and Gökçeada stations were among the stations with a downward trend. From the results, the long-term magnitude of the downward trend among the stations was much lower than the magnitude of the upward trend and the pattern without a trend. Sarıyer station had the strongest upward trend, with a linear regression slope of 0.0715 mm, while Çanakkale station had the strongest long-term downward trend, with a linear regression slope of 0.0092 mm.

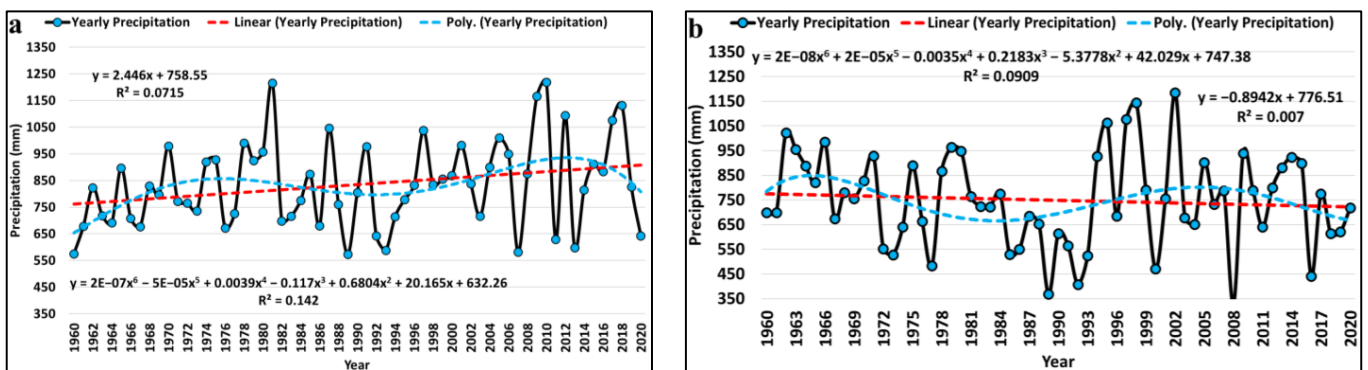


**Figure 4.** The annual time series of precipitation for (a) Sarıyer, (b) Gökçeada stations in the period 1961–2020. We illustrated here the graph of Sarıyer station as a representative of an upward trend and Gökçeada station as a representative of a downward trend.

However, in terms of periodic studies and according to the results of the 6th-order polynomial regression, there were two periods of increasing and decreasing precipitation in the time series at almost all of the stations. The first increasing period was of short duration at most of the stations, started in 1960, and lasted until 1964–1966. After the short-term increasing period, a deep and long-term decreasing trend was observed, except at the Florya, Kocaeli, Kumköy-Kilyos, Sakarya, and Sarıyer stations, which lasted until 1992 (Figure 5a). The periodic trend in precipitation changed after a sharp decrease, and an upward trend was observed in the time series of most stations until 2014–2016. Subsequently, there was a short period of decreasing precipitation fluctuation until the end of 2020. Among the stations in the region, Kocaeli and Sakarya did not follow the classical periodic trend of the other stations and always showed an upward trend both in the long term and periodically (Figure 5b). Bursa had the largest precipitation variation at 881.8 mm.

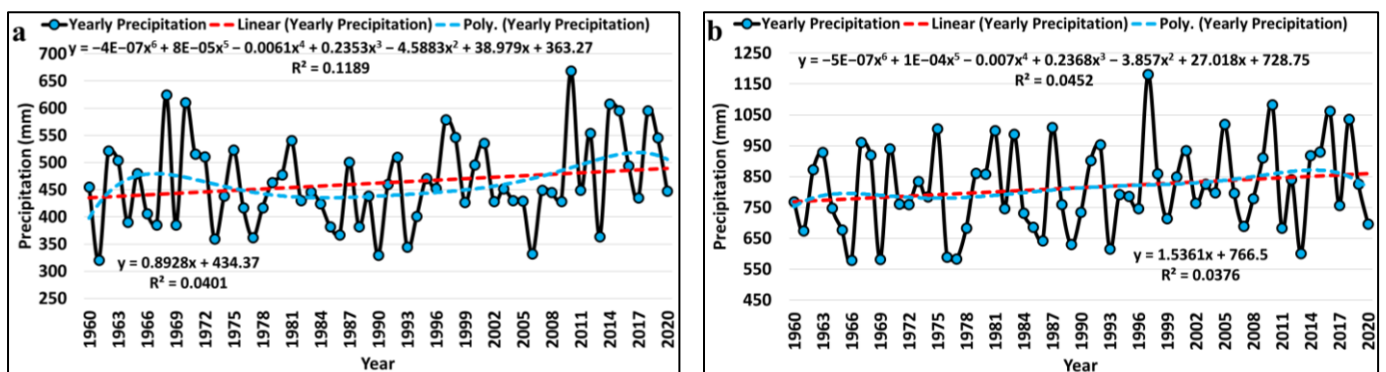


**Figure 5.** The annual time series of precipitation (a) Bilecik, (b) Kocaeli stations in the period 1961–2020. We illustrated here the graph of Bilecik station as a representative of a classical periodic trend and Kocaeli station as a representative of an upward periodic trend.

The precipitation at most stations during the year followed a similar pattern, with the lowest precipitation in summer (July–August) and the highest precipitation in winter (December) (Figure 6a). The precipitation trends throughout the year decreased from January to August and increased from August to December. However, a few stations, including Kocaeli, Sakarya, and Sarıyer, did not follow the general pattern and received almost the same amount of precipitation in spring and summer (Figure 6b).

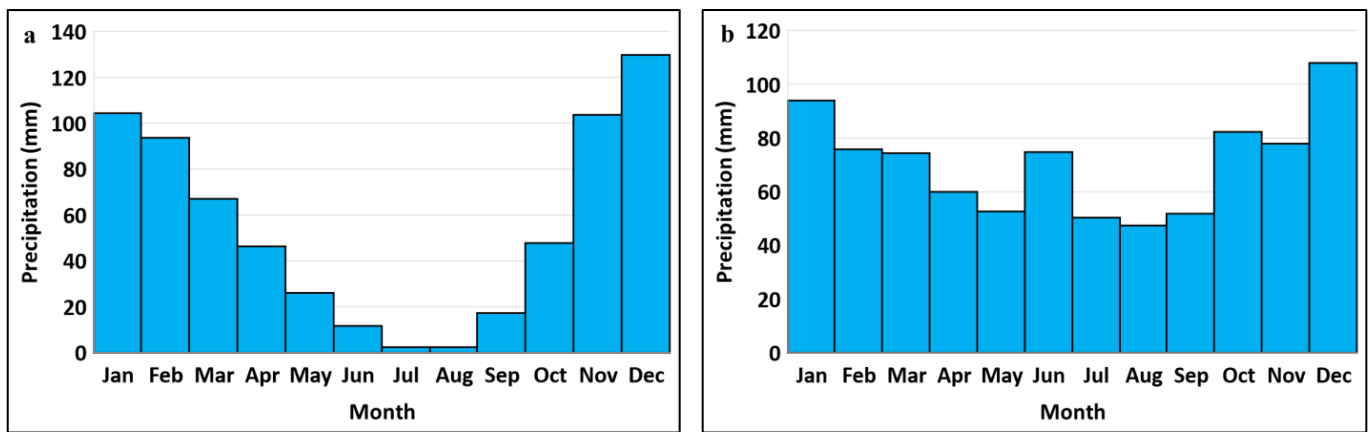


**Figure 6.** The average monthly precipitation amount: (a) Ayvalık, (b) Sakarya stations in the 1961–2020 period. We illustrated here the graph of Ayvalık station as a representative of a classical monthly precipitation distribution and Sakarya station as a representative of a non-classical monthly precipitation distribution.

Moreover, the ombrothermic diagrams of the stations showed that the lowest precipitation and highest temperatures occurred in August and July during the summer. There were six to seven months when the stations had low precipitation and suffered from drought; these conditions were fully observed at eight stations (Figure 7a). However, at some stations, including Edirne and Kırklareli, this period was shorter at approximately four months (Figure 7b). The dry and low precipitation periods started in late March and early April and lasted until September and October.

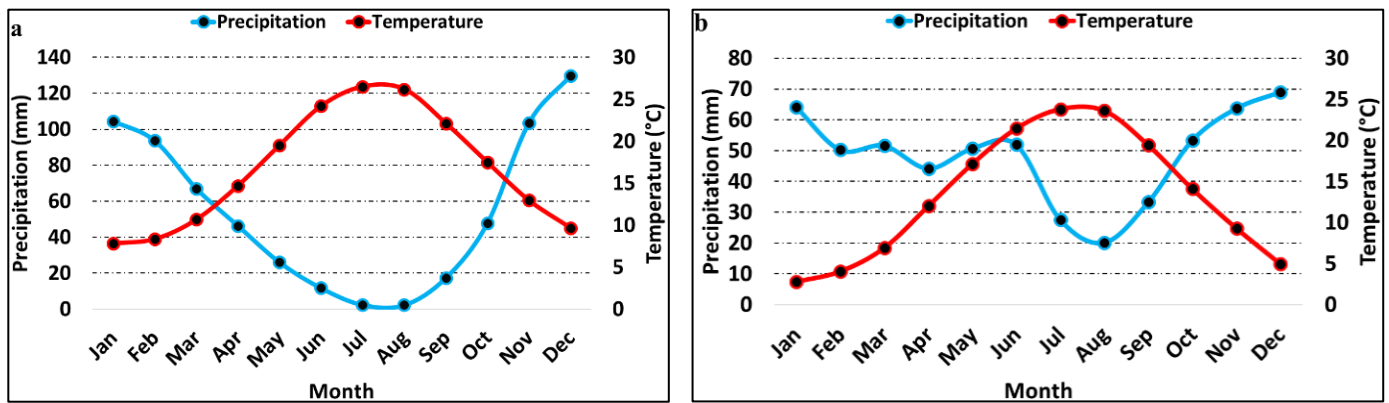


**Figure 7.** The ombrothermic diagram of: (a) Ayvalık, (b) Kırklareli stations in the 1960–2020 period. We illustrated here the graph of Ayvalık station as a representative of a classical conditions of dry and wet months along the year, and Kırklareli station as a representative of a non-classical conditions of dry and wet months along the year.

Based on the hythergraph diagram showing precipitation and temperature variations during the year, it can also be observed that most of the stations had larger precipitation variations than temperature variations. Most stations had long hythergraph diagrams, showing that precipitation variations were larger than temperature variations (Figure 8a). In contrast, at Sarıyer and Kumköy-Kilyos, and to a lesser extent at the Yalova, Tekirdağ, and Kocaeli stations, temperature fluctuations were greater than precipitation (Figure 8b).

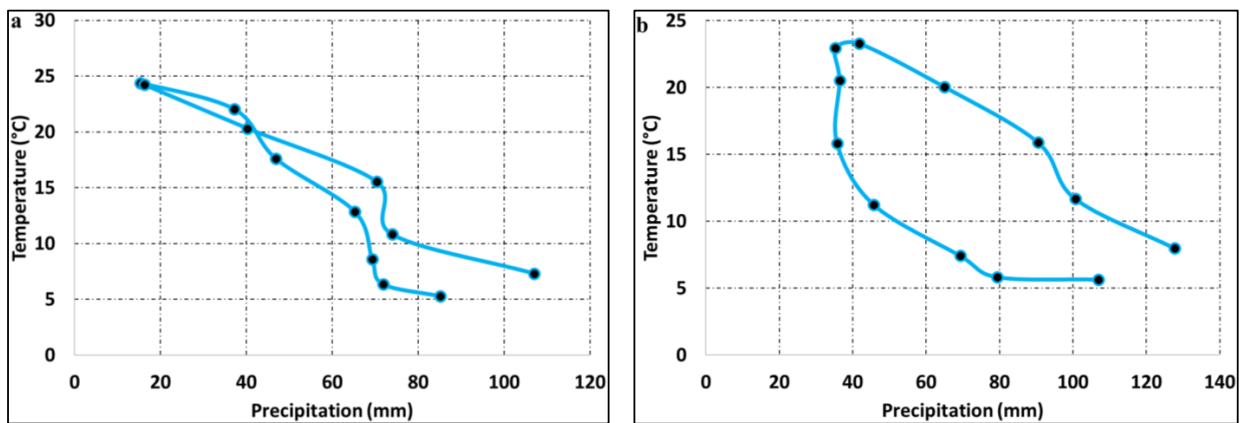


**Figure 8.** The hythergraph diagram of: (a) Bursa, (b) Sarıyer stations in the 1961–2020 period, we illustrated here the graph of Ayvalık station as a representative of a large precipitation variation along the year, and Kırklareli station as a representative of a large temperature variation along the year. In Hythergraph diagram the long graph shows the larger precipitation variation than the temperature and the broader graph shows the vice versa mechanism in the stations.

### 3.3. Man-Kendall Trend Analysis

The Man-Kendall diagrams of most of the stations in the studied area clearly show a downward trend from the beginning of the study period until 1992–1994, and then an upward trend until 2021 (Figure 9a). This phenomenon was observed at approximately 12 out of the 15 stations in the Marmara region. At most stations with this pattern, a sudden mutation in the precipitation time series occurred at the beginning of the study period. In contrast, an opposite and upward trend was formed at Kocaeli, Kumköy-Kilyos, and Sarıyer stations compared to the other stations (Figure 9b). A very important result of the Mann-Kendall test analysis was that the changes in the precipitation trend of most stations (except Bilecik and Kocaeli) were significant. There were significant downward changes at nine stations (Figure 9a), but there were upward at the Kumköy-Kilyos and Sarıyer stations, and to a lesser extent at the Sakarya and Florya stations (Figure 9b). Significant changes in the downward trend occurred during the major decline period between 1960 and 1994. After the end of the decline in 1994, the precipitation levels began to increase at most stations, and sudden changes occurred in the time series. However, since the UI line did not leave a significant range of  $\pm 1.96$ , the changes that occurred in the precipitation trends were not significant.

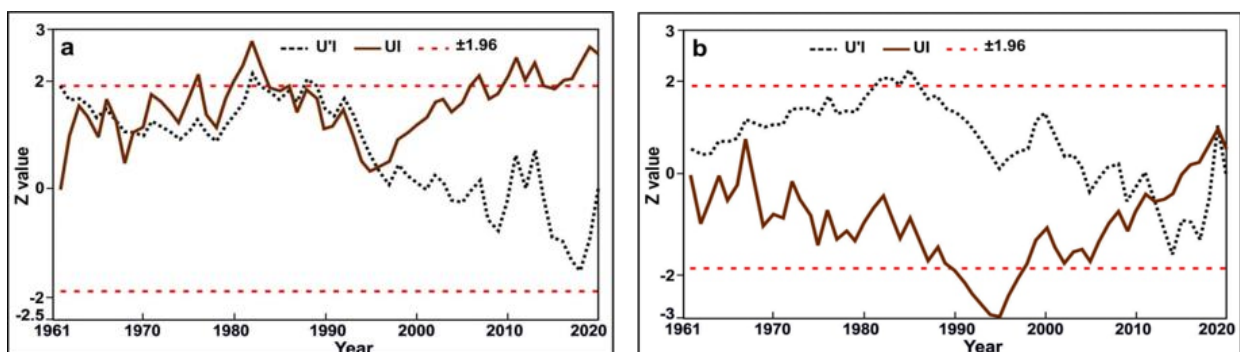


**Figure 9.** The annual Mann-Kendall diagram of: (a) Sarıyer, (b) Edirne stations. We illustrated here the graph of Sarıyer station as a representative of a significant upward trend change, and Edirne station as a representative of a significant downward trend change. Here UI is the observational time series and U'I is the inverse time series.

### 3.4. Precipitation Distribution in the Study Area

#### 3.4.1. Annual Precipitation Distribution

According to Figure 10, the average amount of precipitation in the region ranged from 462 to 850 mm. The largest amount of precipitation occurs in the northeast and north of the Marmara region, and the farther away from this area to the south, southwest, and west, the lower the amount of precipitation. Moreover, Bilecik station and the eastern part of the study area had the lowest precipitation amounts. The further one moves from the coasts, especially the Black Sea coast, towards the inland, the lower the annual precipitation amount in these regions.

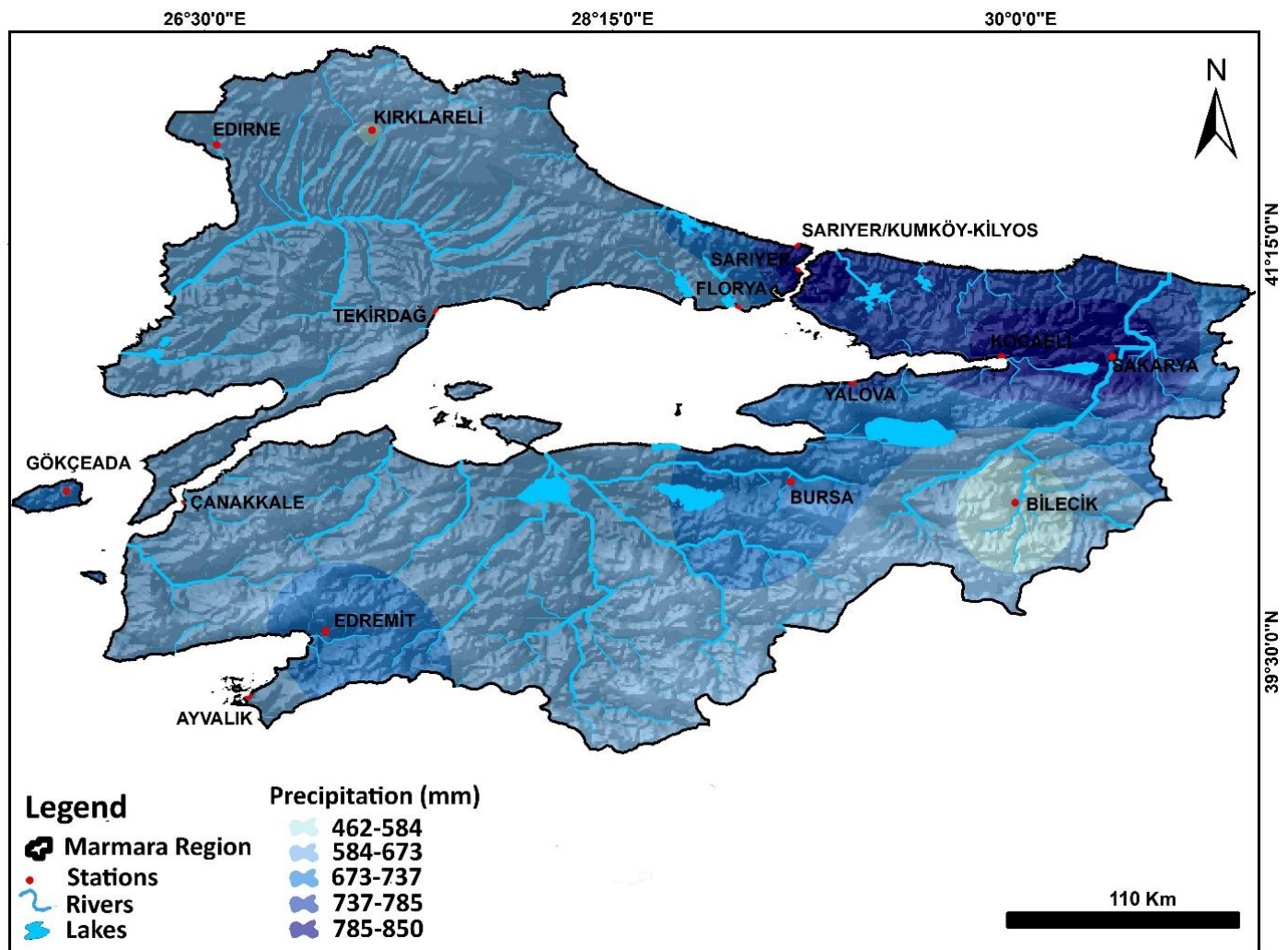
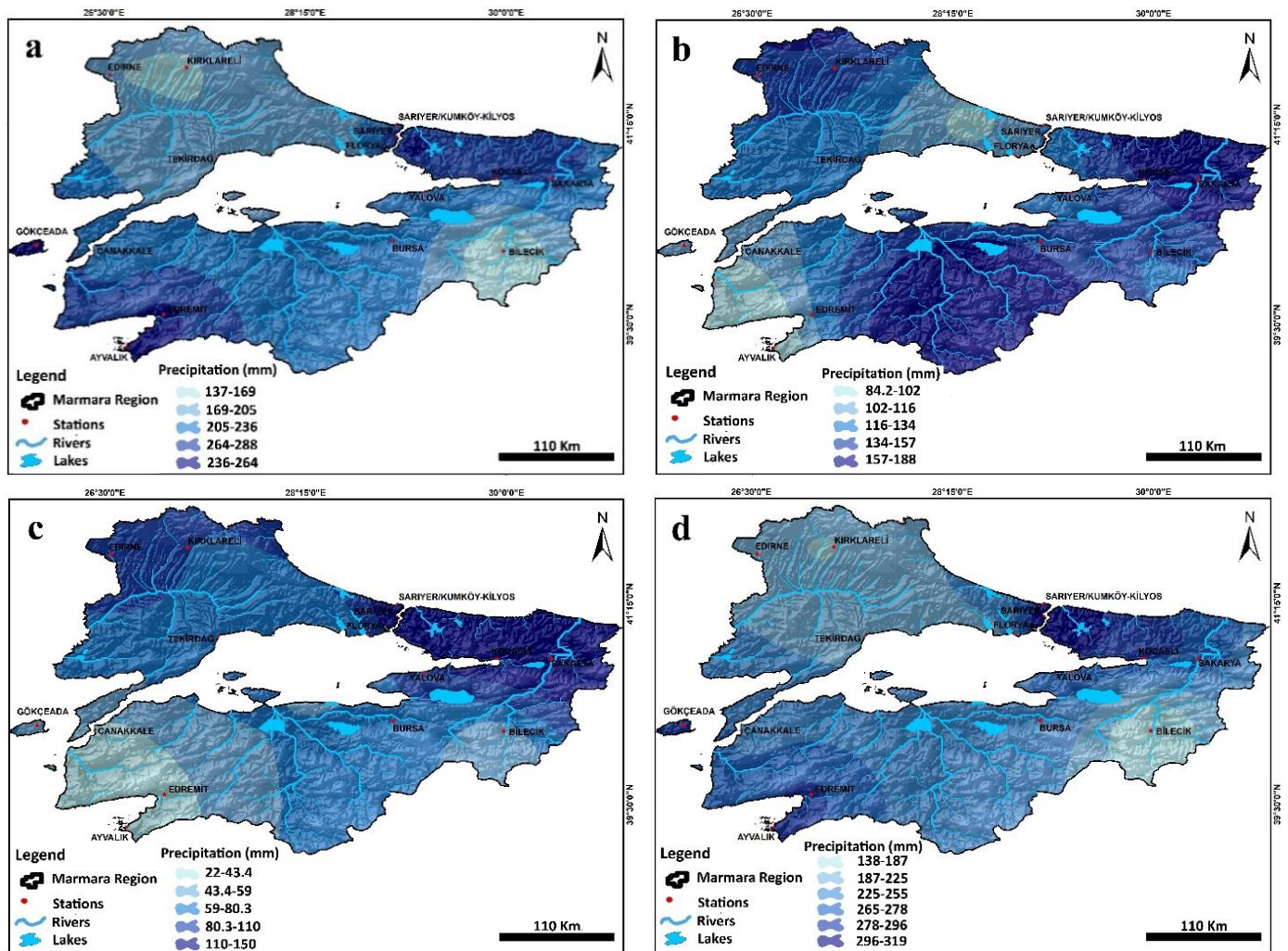


Figure 10. The annual precipitation distribution in the Marmara region.

#### 3.4.2. Seasonal Precipitation Distribution

In winter, most of the precipitation was concentrated in the northeastern and northern regions, including the Black Sea coast, and in the southwestern part of the study area, which includes the coast of the Sea of Marmara. In the aforementioned areas, the highest precipitation amounts occurred in winter, 236–264 mm. In the east of the Marmara region, where the Bilecik station is located, and in the west of the study area, where the Kırklareli station is located, the lowest precipitation amounts (169–137 mm) occurred during this season (Figure 11a). However, in spring, the conditions were somewhat different from those in winter, and the total amount of precipitation was lower. The amount of precipitation during this season varies between 188 and 84.2 mm, and the highest amount was observed in the northeastern regions of the Black Sea coast, northwest, and south of the study area.

However, the lowest amount of precipitation during this season falls in the western part of the Black Sea coast and in the southwestern part of the study area on the coast of the Sea of Marmara (Figure 11b).



**Figure 11.** The seasonal precipitation distribution in the Marmara region: (a) winter, (b) spring, (c) summer, (d) autumn.

In summer, the precipitation in the region reaches a minimum and ranges from 150 to 22 mm. As in the other seasons, the highest amounts of precipitation were recorded on the eastern coast of the Black Sea. In addition, the northwestern part of the study area receives a high amount of precipitation, ranging from 150–110 mm. However, the eastern, southern, and southwestern regions of the study area received the lowest precipitation (80–22 mm) during this season (Figure 11c).

The Marmara region receives the most precipitation in autumn. The highest annual precipitation in this region also occurred in autumn. The average amount of precipitation in autumn ranges from 319 to 138 mm, and the maximum is observed on the Black Sea coasts in the northeast and north of the study area, and on the coast of the Sea of Marmara in the southwest of the region. The lowest amount of precipitation is associated with the Bilecik station in the east of the region. However, the west and northwest also receive less precipitation (225–138 mm) than other areas (Figure 11d).

### 3.5. Exploring the Effects of GLOTI Index

Table 3 shows the percentage of annual and monthly correlations between global temperature and precipitation at the synoptic observation stations. According to the results

of Pearson correlation, only Kocaeli and Sarıyer stations showed positive correlation with global temperature with correlation coefficients of 0.274% and 0.289% and coefficients of determination of 0.075% and 0.084% at a significance level of 0.95%. This shows that global temperature probably has a slightly direct and positive influence on the precipitation at these stations. This means that likely an increase in global temperature leads to an increase in the amount of precipitation and vice versa. Figure 12a,b show the annual relationship plots between global temperature and precipitation for the Sarıyer station.

**Table 3.** Pearson correlation coefficient between global temperature and monthly and annual precipitation of the stations.

Station	Jan	Feb	Mar	Apr	May	Jun	Jul	Aug	Sep	Oct	Nov	Dec	Annually
Ayvalık	0.122	0.010	−0.187	−0.041	−0.020	0.358 **	0.113	−0.048	−0.026	0.347 **	0.023	−0.170	0.085
Bilecik	0.063	0.154	−0.012	−0.022	−0.049	0.335 **	−0.040	−0.188	0.116	0.177	−0.113	−0.016	0.220
Bursa	0.020	0.081	0.050	−0.025	0.171	0.272 *	−0.007	−0.200	0.153	0.225	−0.155	−0.176	0.123
Çanakkale	−0.039	0.066	−0.039	0.036	−0.068	0.208	−0.088	−0.109	−0.076	0.185	−0.010	−0.183	−0.043
Edirne	0.161	0.062	0.048	−0.039	0.078	0.013	0.209	−0.192	0.013	0.286 *	−0.034	−0.059	0.183
Edremit	0.094	0.011	−0.057	−0.036	−0.079	0.098	0.095	−0.152	−0.027	0.304 *	0.031	−0.189	0.018
Florya	−0.021	0.150	0.007	−0.148	0.128	0.121	0.045	−0.112	0.091	0.116	−0.088	−0.194	0.000
Gökçeada	0.087	−0.203	0.007	0.045	0.085	0.186	−0.081	0.006	−0.007	0.197	−0.040	−0.128	−0.011
Kırklareli	0.079	0.024	−0.082	−0.179	0.092	0.186	0.205	−0.153	0.166	0.266 *	−0.014	−0.106	0.139
Kocaeli	0.228	0.122	0.065	0.005	0.218	0.234	0.204	−0.004	−0.051	0.056	−0.100	0.003	0.274 *
Kumköy-Kilyos	−0.049	0.134	−0.054	−0.060	0.005	0.079	0.202	−0.122	0.276 *	0.095	0.037	−0.065	0.131
Sakarya	0.156	0.124	−0.033	0.017	0.303 *	0.172	0.051	−0.067	−0.009	0.091	−0.141	0.012	0.208
Sarıyer	0.049	0.216	0.026	−0.145	0.065	0.288 *	0.127	−0.032	0.245	0.154	0.074	−0.031	0.289 *
Tekirdağ	−0.081	0.146	−0.148	−0.072	−0.006	0.021	0.210	−0.126	0.087	0.274 *	−0.133	−0.142	0.021
Yalova	−0.010	−0.110	−0.086	−0.116	0.223	0.170	−0.084	−0.005	0.029	0.198	0.020	−0.109	0.043

\* 0.95% significant level, \*\* 0.99% significant level.

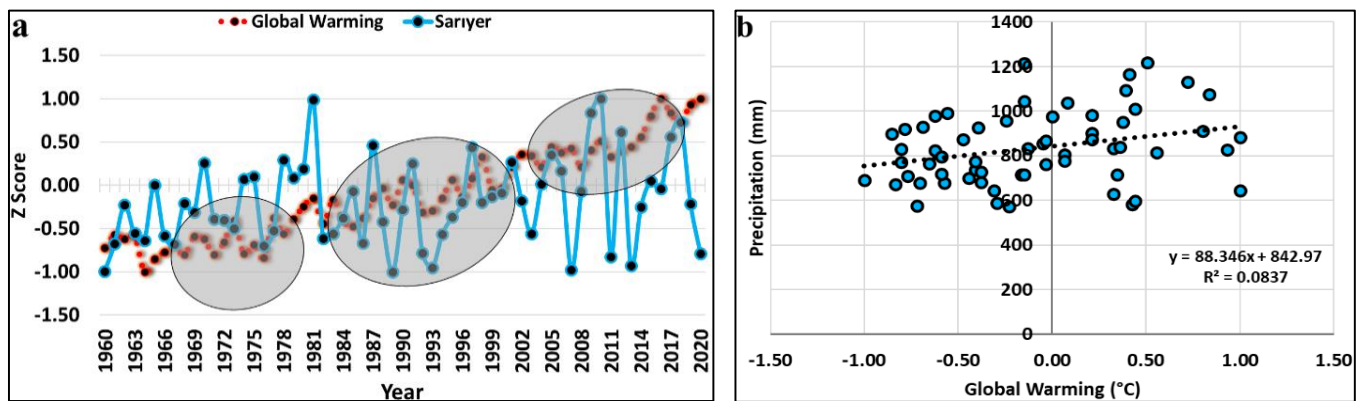


**Figure 12.** The annual relationship graphs between GLOTI index and precipitation for Sarıyer station: (a) standard Z score relationship graph, (b) scatter plot. The grey circles show the period of time that the two data sets have most correlation.

From January to April, there was no relationship between the global temperature and precipitation of the synoptic stations in the region. Only Sakarya station showed a significant correlation with global temperature at the 0.95% significance level in May, with a correlation coefficient of 0.303 and a coefficient of determination of 0.091%. In June, the number of stations correlated with the global temperature increased to four. In this month, the Ayvalık, Bilecik, Bursa, and Sarıyer stations showed a direct positive correlation with global temperature, with correlation coefficients of 0.358, 0.335, 0.272, and 0.288 percent, respectively, and coefficients of determination of 0.13, 0.11, 0.074, and 0.083%, respectively. There was no correlation with global temperature between the stations in July and August. However, in September, only the Kumköy-Kilyos station showed a positive correlation with

global temperature, with significance levels and correlation magnitudes of 0.95 percent and 0.276 percent, respectively.

In autumn, the October precipitation had the highest correlation with global temperature among the months of the year; however, no significant correlation was found in November and December. Five of the stations had a direct positive correlation with the global temperature in October. The Ayvalık station had the highest correlation value, with a correlation value of 0.347% at a significance level of 0.99%. This was followed by Edremit, Edirne, Tekirdağ and Kırklareli stations with correlation coefficients of 0.304, 0.286, 0.274, and 0.266%, respectively. As in the other months, the correlation was positive, indicating that the increase and decrease in global temperature probably caused a direct increase and decrease in precipitation at these stations. Figure 13a,b show the relationship plots of June between the global temperature trend and precipitation at Ayvalık station.

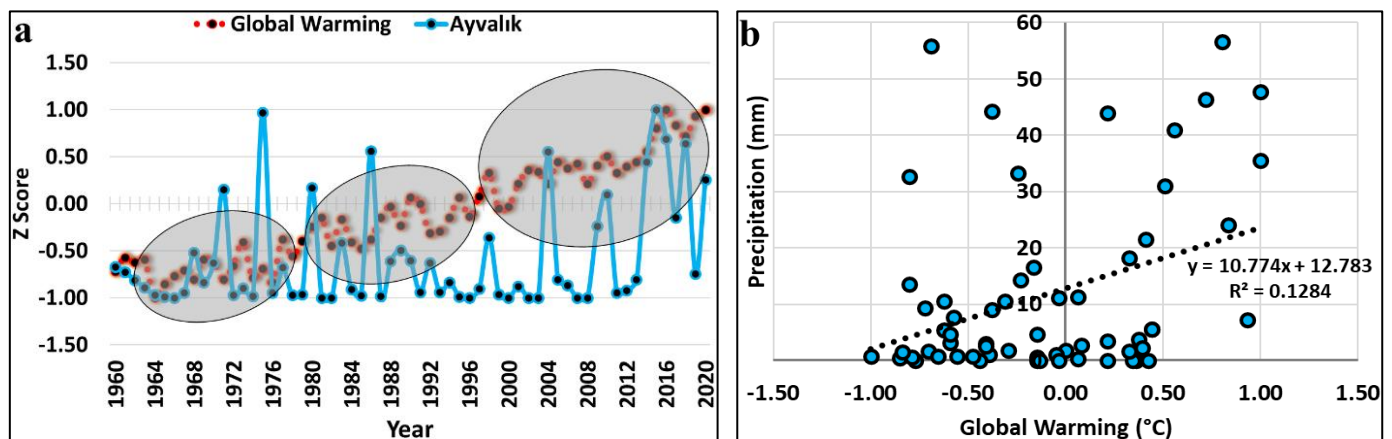


**Figure 13.** The June month relationship graphs between GLOTI index and precipitation of Ayvalık station: (a) standard Z score relation graph, (b) scatter plot. The grey circles show the period of time that the two data sets have most correlation.

### 3.6. Precipitation Modeling with MLP-ANN

For the prediction and modeling of precipitation in the Marmara region, the annual precipitation of the entire region was first determined by averaging the annual precipitation of 15 synoptic stations used in the study. The data were then subjected to a normality test to ensure that they were normally distributed. After determining the annual precipitation in the Marmara region, the predictability of the precipitation variables in the region was evaluated using the R/S method. The Hurst exponent (H) was calculated based on the slope of the curve of the annual precipitation of the entire area. The Hurst exponent in the Marmara region is 0.803. The calculated value of H according to the range of represents the stable behavior of the time series. In such a situation, there is a possibility of repeating the process of the system in a period in the future. A high Hurst curve indicates a high long-term storage effect in a time series [84].

The dynamics and structure of the precipitation time series express the temporal variation in precipitation and influence of various climatic factors. For optimal modeling of precipitation in the region, the most important factors affecting precipitation should be identified and used in the ANN model for simulation and future predictions. For this purpose, nineteen different atmospheric variables that could affect precipitation in the region were used. The specifications of these variables are listed in Table 4. By performing the Pearson correlation test, out of the 19 variables used, only five variables that were significantly correlated with the precipitation amount in the study area were introduced as inputs to the ANN model. The specifications of the selected variables and their correlation coefficients are presented in Table 5.



**Table 4.** The set of climate variables that are considered as input for the model. The time scale of all variables is annual.

Row	Pressure	Humid	Cloud Cover	Sunshine	Temperature	Wind
1	Average	Average	Average	Monthly-Sum	Average	Average
2	Maximum	Maximum	Maximum	Daily Sum-Monthly Ave	Maximum	-
3	Minimum	Minimum	Minimum	-	Minimum	-
4	-	Ave-Max	-	-	Ave-Max	-
5	-	Ave-Min	-	-	Ave-Min	-

**Table 5.** The climatic variables with significant correlation with the annual precipitation in the region.

Variables	Ave-Pressure	Ave-Temp	Min/Ave-Temp	Max-Cloud	Ave-Humid
Correlation	-0.482 **	0.28 *	0.312 *	0.281 *	0.301 *

\* 0.95 Significant level, \*\* 0.99 Significant level.

Table 5 shows that, with the exception of the variable of average pressure, which has a negative correlation with precipitation in the region with a significance level of 0.99%, the remaining variables have a positive correlation with a significance level of 0.95%. Among the variables that have a positive correlation with regional precipitation, the variable of average minimum temperature with 0.312% has the highest correlation coefficient. The variables average humidity with 0.301, maximum cloudy days with 0.281 and average temperature with 0.28 correlation coefficient are in the following categories. The ANN model used in this study is a three-layer perceptron network using backpropagation training (BP) along with the BFGS learning algorithm. It should be noted that the learning algorithm used had the lowest error rate compared to other MLP algorithms in precipitation modeling of the Marmara region with five defined input layers. The topology as well as the characteristics of the ANN used are shown in Figure 14 and Table 6.

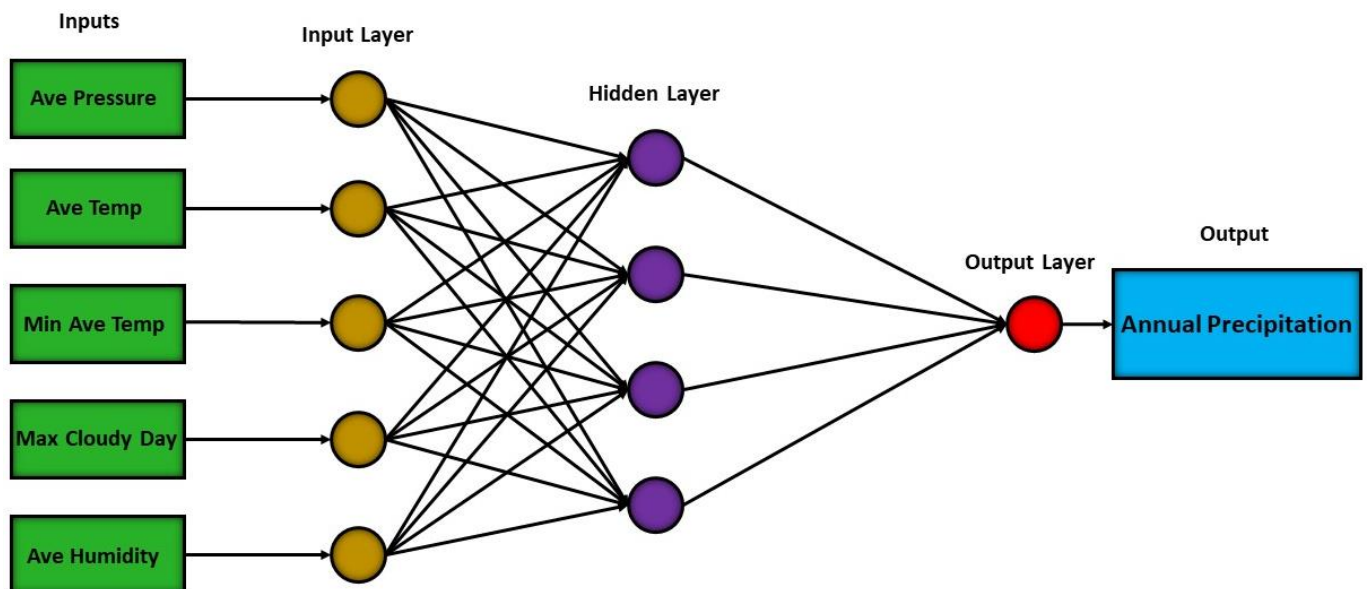


**Figure 14.** The topology of the developed ANN.

**Table 6.** The characteristics of the developed ANN model.

Name	Hidden Layer	Number of Neuron	Training Algorithm	Error Function	Hidden Activation	Output Activation
MLP	1	4	BFGS	SOS	Exponential	Tanh

The BFGS training algorithm of the MLP-ANN was used to establish, train, validate, and test the efficiency of predicting the actual precipitation in the Marmara region based on five climate variables. Seventy percent of the sixty-one yearly in situ data points were used to train the network, 15 percent were used for validation to check the overfitting tendency of the network, and the remaining 15 percent were used to test the accuracy of the ANN models.

The results of the precipitation modeling in the Marmara region by MLP-ANN using the BFGS algorithm are shown in Figures 15–17. According to the results, the selected ANN model simulated actual precipitation in the Marmara region. Looking at the scatter plot showing the correlation between the actual precipitation values in the area and the values predicted by the ANN model, the R2 value of this model was 0.778%. From Figures 15 and 17, it can be seen that the simulation of the real precipitation in the Marmara region by the developed ANN model has been well performed, which is especially evident for the period from 1999 to 2021.

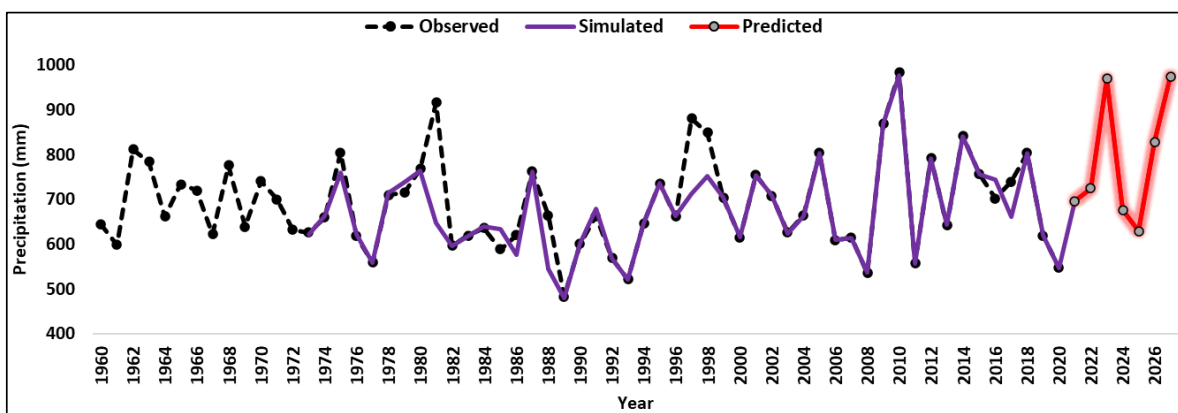


Figure 15. The time series plot of annual precipitation in Marmara region and simulated/predicted precipitation amount by the developed ANN.

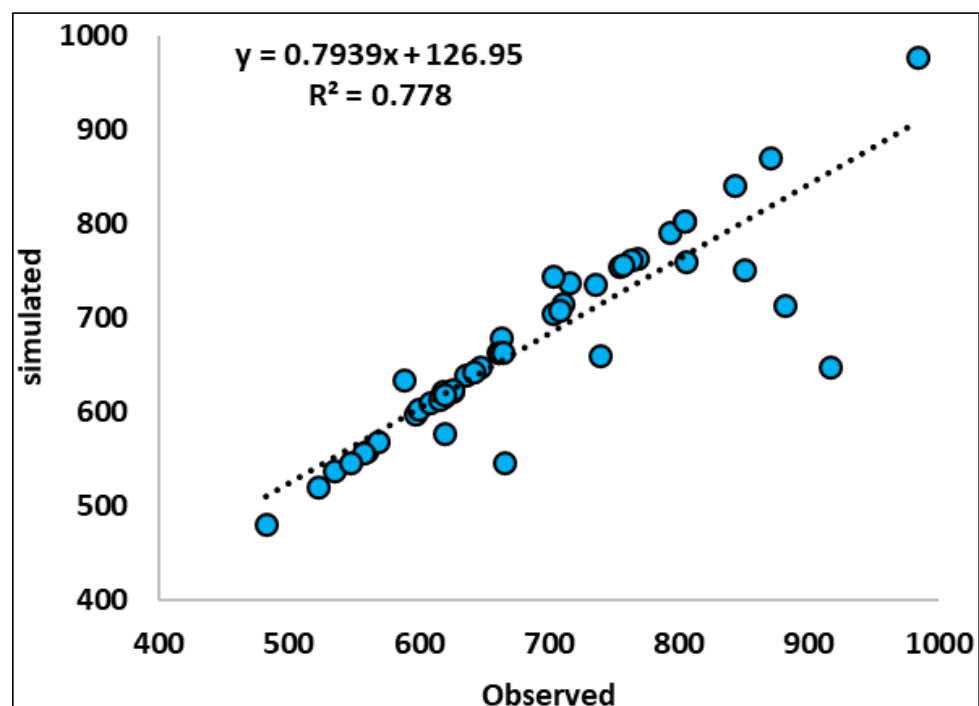
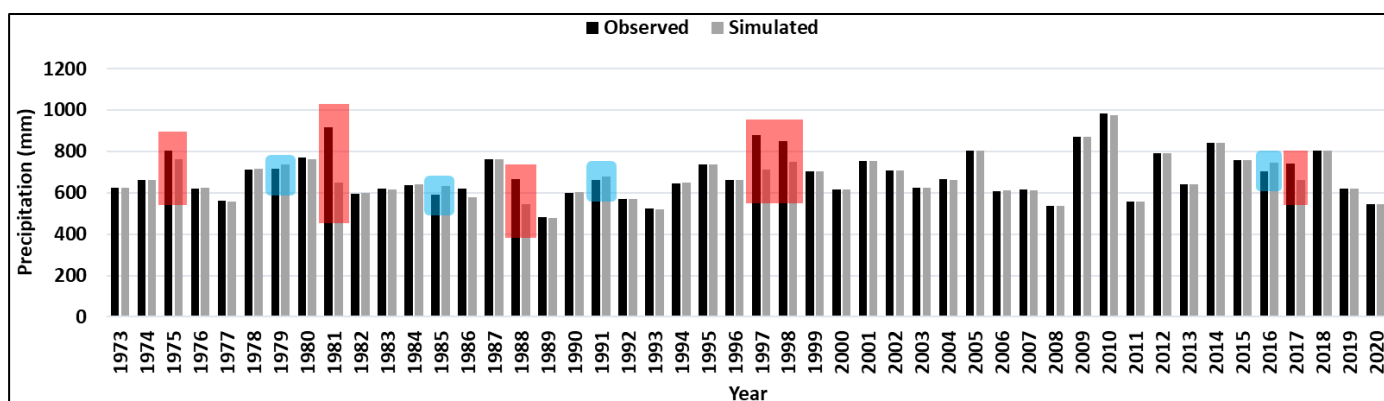


Figure 16. The scatter plot of the observed and simulated precipitation amount by the developed ANN.



**Figure 17.** The graph of differences between simulated and observed precipitation in the Marmara region between 1973 and 2020. Here the red boxes are the significantly underestimated and the blue boxes are the significant overestimated amount of precipitation with the developed MLP-ANN model.

The actual amount of precipitation in the region was significantly overestimated four times by the ANN model, with the highest value of 44.2 mm 1985. However, the actual amount of precipitation was significantly underestimated five times, with the highest value recorded in 1981 at 268.11 mm (Figure 17). The prediction of precipitation amount by the developed ANN model until 2027 showed an upward trend in the future. The maximum predicted precipitation is 974 mm in 2027, and the minimum predicted amount is 629 mm in 2025. In general, the upward scenario predicted by the ANN was consistent and fully compatible with the general precipitation trend in the Marmara region during the last 61 years.

#### 4. Discussion

According to the time series analyses, the long-term trend of precipitation in the weather stations of the Marmara region in Turkey does not follow a constant pattern, and there is either an upward trend, a downward trend, or no trend in the long-term time series of these stations. These results are in agreement with results of previous studies [85–89]. However, the noteworthy point in this regard is the superiority of the upward and trendless pattern compared to the downward trend of precipitation in the stations, which indicates almost no downward slope of precipitation in the entire region during the past 61 years. Among the stations, six stations have experienced no trend, six stations have experienced an upward trend, and three stations have experienced a downward trend in their long-term time series. In terms of analyzing the periodic trend of precipitation at the stations of the Marmara region, two downward and upward periods can be identified in the 61-year time series. However, 2 out of the total of 15 stations in the region did not follow this trend and have always experienced an upward trend in the long term. The upward periods of precipitation among the stations were mostly short-term upward periods (from 1960 to 1964–1966) and long-term upward periods (from 1992 to 2014–2016), and the downward periods also included a long-term downward period (from 1964–1966 to 1992) and a short-term downward period (from 2014–2016 to 2020). The mentioned ascending and descending periods are consistent with the results of the study on the precipitation trend in Greece [90]. The results of the time series analysis section contradict the findings of some researchers [26,86,90–94] who suggested a decreasing trend in precipitation in the Eastern Mediterranean regions, while on the other hand, it is consistent with the results of some researchers [36,95] who proposed an upward trend and no trend in precipitation in the long term in the region.

The monthly and seasonal precipitation distribution among the studied stations follows the pattern of Mediterranean precipitation distribution [96] that can be described as minimum amount of precipitation in the summer and the maximum amount in late autumn

and winter. The stations in the study area experience four-seven months of precipitation stress and suffer from a lack of precipitation. This has led to evident changes in precipitation compared to temperature which is well demonstrated by analyzing the ombrothermic and hythergraph charts of the stations. The research conducted by [30] confirms the results of this study.

The Mann-Kendall trend analysis method is also one of the common methods that has been widely used by researchers in various fields to investigate trends in time series data, especially in meteorological data [46–50]. Despite the advantages of this method, which has a high ability to identify monotonic trends of a variable and is faster than parametric methods, its results may not be reliable for the data with seasonal and serial correlation [44,45]. The Mann-Kendall trend test indicates the presence of a trend in the precipitation data for the stations except for the Bilecik and Kocaeli stations. The trend observed at the beginning of the time series in most stations is a long-term downward trend. This long-term decreasing trend has been observed in 12 stations and in 9 of these stations, the change in trend has been statistically significant with the departure of the UI line from the significance threshold of  $\pm 1.96\%$ . The period in which the significant change in the decreasing trend occurred among the stations was between 1989 and 1995. After this period, the decreasing trend transformed into an ascending one until the end of the study period, which is not statistically significant. On the other hand, the time of the onset of this sudden change in trend, which led to a decreasing mutation in the precipitation trend of the stations, was between 1965 and 1972, which can be considered as the start of the decreasing trend in the stations. However, in the three stations of Kocaeli, Kumköy-Kilyos, and Sarıyer, the initial trend has been upward, and except for the Kocaeli station, in the remaining two stations located in the Bosphorus area of Istanbul, this upward trend has been statistically significant. This may be as a result of air masses that affect this part of the study area and lead to the formation of a different pattern compared to other stations in the region [85]. These results are consistent with the results in [85,86,91,92,97,98], and contradict the results of studies by [88,89].

The annual precipitation in the region was analyzed and it was found that the north-east of the Marmara Region that is influenced by the Black Sea, and the central parts of Istanbul that includes Bosphorus receive the greatest amount of precipitation. The annual precipitation decreases by moving away from these areas and in the eastern regions that are distant from the coasts, it reaches its minimum level. These findings are in line with those of the study conducted by [99]. The spatial distribution of total precipitation has the same pattern for all seasons. This can be attributed to the impact of air masses that originate from the north, travel over the Black Sea, and carry a considerable amount of moisture before reaching these areas. This leads to a higher precipitation amount compared to other regions. Since the air mass penetrating the region loses its highest moisture content in the coasts and slopes facing the northern highlands, areas far from the coastline receive less precipitation. Among these areas, the eastern parts of the region are the areas with the lowest precipitation, as reported in the studies by [100,101].

The impact of global temperature fluctuations on precipitation of the stations has been limited but positive. Only two stations, Kocaeli and Sarıyer, had a positive correlation with global temperature changes for the annual precipitation during 61 years. The correlation between temperature fluctuations and precipitation has also been limited on a monthly basis, with the maximum observed between the stations in October. It should be noted that the results obtained in this study are based on the direct correlation between global temperature and precipitation at the investigated stations in the region. Investigating the indirect effect, as well as the delayed effect of these two parameters on precipitation, may yield interesting and significant results. However, such analysis is beyond the scope of this study and will be addressed in further studies.

The neural network model developed in this study was able to simulate the amount of precipitation in the region well, as evident from the results, and provided an acceptable prediction. The ANN model is widely recognized as a powerful tool for simulating and

predicting weather parameters, with a particular emphasis on precipitation. This model has been utilized by numerous atmospheric science researchers and has consistently produced satisfactory results, as demonstrated by studies such as those conducted by [102–106]. The MLP-ANN developed in this study accurately predicted the total precipitation in the Marmara region with an R<sup>2</sup> value of 0.778. Furthermore, the prediction for the period up to 2027 indicates an increasing trend of precipitation in the region in the upcoming years, consistent with the time series analysis of the region's stations over a 61-year period.

## 5. Conclusions

The present study was conducted to investigate the past, present, and future situation of precipitation in the Marmara region of Türkiye over 61 years (1960–2020). The analysis showed that during the study period, the upward and zero trends were superior to the downward trend in the time series of precipitation over the long term. However, in the short term, the precipitation trends at the stations were different, and two periods of decreasing and increasing precipitation were observed at most stations. The longest period of decreasing precipitation generally began between 1964 and 1965 and lasted until 1992. By contrast, the longest upward trend began in 1992 and lasted from 2014 to 2016. During the year, the precipitation trend decreased from January to July–August and increased from August to January, and the lowest amount of precipitation fell first in summer and then in spring. In general, the stations in the study area experienced low precipitation and drought for a maximum of six–seven months during the year, and the precipitation changes and variations in the region were stronger than the temperature. The trend analysis performed by the Mann-Kendall method showed that out of the 15 stations in the region, 13 stations had a significant change in the time series trend of precipitation. This significant change in precipitation occurred during a period of sharp precipitation decline in the 1990s. The 61-year distribution of precipitation throughout the region showed that the highest precipitation amounts were recorded in the northeast of the study area along the southeastern coast of the Black Sea and northeastern coast of the Sea of Marmara. The lowest precipitation amounts were recorded mainly in the eastern areas of the region around Bilecik station. This indicates that the amount of precipitation decreases as one moves away from the moisture sources.

The study of the effects of the global warling index (ILOTI index) on the precipitation amounts at the stations in the Marmara region showed a small positive influence of this index on the precipitation trend. In the annual dimension, only two stations showed a positive correlation with global temperature, and among the months of the year, October showed the highest positive correlation with five stations. The results of the simulation and prediction of precipitation in the Marmara region using the ANN model show acceptable accuracy of the modeling and illustrate an upward scenario for precipitation in this region until 2027.

**Author Contributions:** Conceptualization, M.A. and A.K. (Atilla Karataş); methodology, M.A.; investigation, M.A.; writing—original draft preparation, M.A.; writing—review and editing, M.A., A.K. (Atilla Karataş), A.R.L., B.E. and A.K. (Azra Khosravichenar); visualization, M.A. and A.K. (Atilla Karataş). All authors have read and agreed to the published version of the manuscript.

**Funding:** This research received no external funding.

**Institutional Review Board Statement:** Not applicable.

**Informed Consent Statement:** Not applicable.

**Data Availability Statement:** The data supporting the findings of this study are available upon reasonable request from the authors.

**Acknowledgments:** The authors would like to thank the Turkish Meteorological Organization for providing access to meteorological data from the Marmara region stations. The authors acknowledge the role of the anonymous reviewer and the editor-in-chief who helped strengthen this work. The authors wish to express their gratitude to the Leipzig University authorities for generously covering the publication fee for this paper.

**Conflicts of Interest:** The authors declare that they have no conflict of interest.

## References

1. Frederick, K.D.; Major, D.C. Climate change and water resources. *Clim. Chang.* **1997**, *37*, 7–23. [[CrossRef](#)]
2. Kansakar, S.R.; Hannah, D.M.; Gerrard, J.; Rees, G. Spatial pattern in the precipitation regime of Nepal. *Int. J. Climatol. A J. R. Meteorol. Soc.* **2004**, *24*, 1645–1659. [[CrossRef](#)]
3. Xoplaki, E.; González-Rouco, J.F.; Luterbacher, J.; Wanner, H. Wet season Mediterranean precipitation variability: Influence of large-scale dynamics and trends. *Clim. Dyn.* **2004**, *23*, 63–78. [[CrossRef](#)]
4. López-Díaz, F.; Conde, C.; Sánchez, O. Analysis of indices of extreme temperature events at Apizaco, Tlaxcala, Mexico: 1952–2003. *Atmósfera* **2013**, *26*, 349–358. [[CrossRef](#)]
5. Chen, S.; Hu, J.; Zhang, A.; Min, C.; Huang, C.; Liang, Z. Performance of near real-time Global Satellite Mapping of Precipitation estimates during heavy precipitation events over northern China. *Theor. Appl. Climatol.* **2019**, *135*, 877–891. [[CrossRef](#)]
6. Aalijahan, M.; Khosravichenar, A. A multimethod analysis for average annual precipitation mapping in the Khorasan Razavi Province (Northeastern Iran). *Atmosphere* **2021**, *12*, 592. [[CrossRef](#)]
7. Aalijahan, M.; Lupo, A.R.; Salahi, B.; Rahimi, Y.G.; Asl, M.F. The long-term (142 years) spatiotemporal reconstruction and synoptic analysis of extreme low temperatures ( $-15\text{ }^{\circ}\text{C}$  or lower) in the northwest region of Iran. *Theor. Appl. Climatol.* **2022**, *147*, 1415–1436. [[CrossRef](#)]
8. Pachauri, R.K.; Reisinger, A. *IPCC Fourth Assessment Report*; IPCC: Geneva, Switzerland, 2007.
9. Hartmann, D.L.; Klein Tank, A.M.G.; Rusticucci, M.; Alexander, L.V.; Brönnimann, S.; Charabi, Y.; Dentener, F.J.; Dlugokencky, E.J.; Easterling, D.R.; Kaplan, A.; et al. Observations: Atmosphere and surface. In *Climate Change 2013 the Physical Science Basis: Working Group I Contribution to the Fifth Assessment Report of the Intergovernmental Panel on Climate Change*; Cambridge University Press: Cambridge, UK, 2013; pp. 159–254.
10. Allan, R.P.; Soden, B.J. Atmospheric warming and the amplification of precipitation extremes. *Science* **2008**, *321*, 1481–1484. [[CrossRef](#)]
11. Min, S.K.; Zhang, X.; Zwiers, F.W.; Hegerl, G.C. Human contribution to more-intense precipitation extremes. *Nature* **2011**, *470*, 378–381. [[CrossRef](#)] [[PubMed](#)]
12. Shiu, C.J.; Liu, S.C.; Fu, C.; Dai, A.; Sun, Y. How much do precipitation extremes change in a warming climate? *Geophys. Res. Lett.* **2012**, *39*. [[CrossRef](#)]
13. Field, C.B.; Barros, V.; Stocker, T.F.; Dahe, Q. (Eds.) *Managing the Risks of Extreme Events and Disasters to Advance Climate Change Adaptation: Special Report of the Intergovernmental Panel on Climate Change*; Cambridge University Press: Cambridge, UK, 2012.
14. Asadieh, B.; Krakauer, N.Y. Global trends in extreme precipitation: Climate models versus observations. *Hydrol. Earth Syst. Sci.* **2015**, *19*, 877–891. [[CrossRef](#)]
15. Champion, A.J.; Blenkinsop, S.; Li, X.F.; Fowler, H.J. Synoptic-scale precursors of extreme UK summer 3-hourly rainfall. *J. Geophys. Res. Atmos.* **2019**, *124*, 4477–4489. [[CrossRef](#)]
16. Margiorou, S.; Kastridis, A.; Sapountzis, M. Pre/Post-Fire Soil Erosion and Evaluation of Check-Dams Effectiveness in Mediterranean Suburban Catchments Based on Field Measurements and Modeling. *Land* **2022**, *11*, 1705. [[CrossRef](#)]
17. Pastor, A.V.; Nunes, J.P.; Ciampalini, R.; Koopmans, M.; Baartman, J.; Huard, F.; Calheiros, T.; Le-Bissonnais, Y.; Keizer, J.J.; Raclot, D. Projecting future impacts of global change including fires on soil erosion to anticipate better land management in the forests of NW Portugal. *Water* **2019**, *11*, 2617. [[CrossRef](#)]
18. Westra, S.; Alexander, L.V.; Zwiers, F.W. Global increasing trends in annual maximum daily precipitation. *J. Clim.* **2013**, *26*, 3904–3918. [[CrossRef](#)]
19. Bocheva, L.; Pophristov, V. Seasonal analysis of large-scale heavy precipitation events in Bulgaria. In *AIP Conference Proceedings*; AIP Publishing LLC: Melville, NY, USA, 2019; Volume 2075, p. 200017.
20. Solomon, S.; Manning, M.; Marquis, M.; Qin, D. *Climate Change 2007-the Physical Science Basis: Working Group I Contribution to the Fourth Assessment Report of the IPCC*; Cambridge University Press: Cambridge, UK, 2007; Volume 4.
21. Pachauri, R.K.; Allen, M.R.; Barros, V.R.; Broome, J.; Cramer, W.; Christ, R.; Church, J.A.; Clarke, L.; Dahe, Q.; Dasgupta, P.; et al. *Climate Change 2014: Synthesis Report. Contribution of Working Groups I, II and III to the Fifth Assessment Report of the Intergovernmental Panel on Climate Change*; IPCC: Geneva, Switzerland, 2014; p. 151.
22. Giorgi, F.; Lionello, P. Climate change projections for the Mediterranean region. *Glob. Planet. Chang.* **2008**, *63*, 90–104. [[CrossRef](#)]
23. Palutikof, J.P.; Trigo, R.M.; Adcock, S.T. Scenarios of future rainfall over the Mediterranean: Is the region drying. In *Proceedings of the Mediterranean Desertification, Research Results and Policy Implications, Crete, Greece, 29 October–1 November 1996*; Volume 20, pp. 33–39.

24. Piervitali, E.; Colacino, M.; Conte, M. Signals of climatic change in the central-western Mediterranean basin. *Theor. Appl. Climatol.* **1997**, *58*, 211–219. [[CrossRef](#)]
25. Norrant, C.; Douguédroit, A. Monthly and daily precipitation trends in the Mediterranean (1950–2000). *Theor. Appl. Climatol.* **2006**, *83*, 89–106. [[CrossRef](#)]
26. Philandras, C.M.; Nastos, P.T.; Kapsomenakis, J.; Douvis, K.C.; Tselioudis, G.; Zerefos, C.S. Long term precipitation trends and variability within the Mediterranean region. *Nat. Hazards Earth Syst. Sci.* **2011**, *11*, 3235–3250. [[CrossRef](#)]
27. Alexandrov, V.; Schneider, M.; Koleva, E.; Moisselin, J.M. Climate variability and change in Bulgaria during the 20th century. *Theor. Appl. Climatol.* **2004**, *79*, 133–149. [[CrossRef](#)]
28. Tomozeiu, R.; Stefan, S.; Busuioc, A. Winter precipitation variability and large-scale circulation patterns in Romania. *Theor. Appl. Climatol.* **2005**, *81*, 193–201. [[CrossRef](#)]
29. Feidas, H.; Nouloupoulou, C.; Makrogiannis, T.; Bora-Senta, E. Trend analysis of precipitation time series in Greece and their relationship with circulation using surface and satellite data: 1955–2001. *Theor. Appl. Climatol.* **2007**, *87*, 155–177. [[CrossRef](#)]
30. Gönençgil, B.; İçel, G. Variations of total yearly precipitation in Eastern Mediterranean coasts of Turkey (1975–2006). *Türk. Coğrafya Derg.* **2010**, *55*, 2014. (In Turkish)
31. Partal, T.; Kahya, E. Trend analysis in Turkish precipitation data. *Hydrol. Process. Int. J.* **2006**, *20*, 2011–2026. [[CrossRef](#)]
32. Tayanç, M.; Im, U.; Doğruel, M.; Karaca, M. Climate change in Turkey for the last half century. *Clim. Chang.* **2009**, *94*, 483–502. [[CrossRef](#)]
33. Türkes, M. Spatial and temporal analysis of annual rainfall variations in Turkey. *Int. J. Climatol. A J. R. Meteorol. Soc.* **1996**, *16*, 1057–1076. [[CrossRef](#)]
34. Özhan, S. *Watershed Management*; Publication No. 481; Istanbul University: Istanbul, Türkiye, 2004. (In Turkish)
35. Atalay, I. *Applied Climatology*; META Basım Printing Services: Bornova, Türkiye, 2010. (In Turkish)
36. Abbasnia, M.; Toros, H. Analysis of Long-Term Changes in Extreme Climatic Indices: A Case Study of the Mediterranean Climate, Marmara Region, Turkey. In *Meteorology and Climatology of the Mediterranean and Black Seas*; Springer Nature: Cham, Switzerland, 2019; pp. 141–153.
37. Babai-Fini, O.M.; Najafpour, B. *Climate Maps and Diagrams*; Payam Noor University: Tehran, Iran, 2014.
38. Farajzadeh Asl, M. *Climatology Techniques*; Samt: Tehran, Iran, 2015. (In Persian)
39. Lanzante, J.R. Resistant, robust and non-parametric techniques for the analysis of climate data: Theory and examples, including applications to historical radiosonde station data. *Int. J. Climatol. A J. R. Meteorol. Soc.* **1996**, *16*, 1197–1226. [[CrossRef](#)]
40. Davis, J.C.; Sampson, R.J. *Statistics and Data Analysis in Geology*; Wiley: New York, NY, USA, 1986; Volume 646.
41. Rossi, R.E.; Mulla, D.J.; Journel, A.G.; Franz, E.H. Geostatistical tools for modeling and interpreting ecological spatial dependence. *Ecol. Monogr.* **1992**, *62*, 277–314. [[CrossRef](#)]
42. Yadav, R.; Tripathi, S.K.; Pranuthi, G.; Dubey, S.K. Trend analysis by Mann-Kendall test for precipitation and temperature for thirteen districts of Uttarakhand. *J. Agrometeorol.* **2014**, *16*, 164. [[CrossRef](#)]
43. Pohlert, T. Non-parametric trend tests and change-point detection. *CC BY-ND* **2016**, *4*, 1–18.
44. Zaghoul, M.S.; Ghaderpour, E.; Dastour, H.; Farjad, B.; Gupta, A.; Eum, H.; Achari, G.; Hassan, Q.K. Long-Term Trend Analysis of River Flow and Climate in Northern Canada. *Hydrology* **2022**, *9*, 197. [[CrossRef](#)]
45. Shawky, M.; Ahmed, M.R.; Ghaderpour, E.; Gupta, A.; Achari, G.; Dewan, A.; Hassan, Q.K. Remote sensing-derived land surface temperature trends over South Asia. *Ecol. Inform.* **2023**, *74*, 101969. [[CrossRef](#)]
46. Li, L.J.; Zhang, L.; Wang, H.; Wang, J.; Yang, J.W.; Jiang, D.J.; Li, J.Y.; Qin, D.Y. Assessing the impact of climate variability and human activities on streamflow from the Wuding River basin in China. *Hydrol. Process. Int. J.* **2007**, *21*, 3485–3491. [[CrossRef](#)]
47. Tian, F.; Yang, Y.; Han, S. Using runoff slope-break to determine dominant factors of runoff decline in Hutuo River Basin, North China. *Water Sci. Technol.* **2009**, *60*, 2135–2144. [[CrossRef](#)] [[PubMed](#)]
48. Ye, X.; Zhang, Q.; Liu, J.; Li, X.; Xu, C.Y. Distinguishing the relative impacts of climate change and human activities on variation of streamflow in the Poyang Lake catchment, China. *J. Hydrol.* **2013**, *494*, 83–95. [[CrossRef](#)]
49. Zhang, X.; Li, P.; Li, D. Spatiotemporal variations of precipitation in the southern part of the Heihe river basin (China), 1984–2014. *Water* **2018**, *10*, 410. [[CrossRef](#)]
50. Efe, B.; Gözet, E.; Özgür, E.; Lupo, A.R.; Deniz, A. Spatiotemporal Variation of Tourism Climate Index for Türkiye during 1981–2020. *Climate* **2022**, *10*, 151. [[CrossRef](#)]
51. Liu, J.; Xue, B.; Sun, W.; Guo, Q. Water balance changes in response to climate change in the upper Hailar River Basin, China. *Hydrol. Res.* **2020**, *51*, 1023–1035. [[CrossRef](#)]
52. Feyzi, V. Analysis of Spatial-Temporal Distribution of Climate Change in Iran. Master's Thesis, Faculty of Literature and Humanities, Department of Physical Geography, Tarbiat Modares University, Tehran, Iran, 2009. (In Persian).
53. Wang, W.; Van Gelder, P.H.; Vrijling, J.K.; Ma, J. Forecasting daily streamflow using hybrid ANN models. *J. Hydrol.* **2006**, *324*, 383–399. [[CrossRef](#)]
54. Alberto Meda-Campana, J. On the estimation and control of nonlinear systems with parametric uncertainties and noisy outputs. *IEEE Access* **2018**, *6*, 31968–31973. [[CrossRef](#)]
55. Chiang, H.S.; Chen, M.Y.; Huang, Y.J. Wavelet-based EEG processing for epilepsy detection using fuzzy entropy and associative petri net. *IEEE Access* **2019**, *7*, 103255–103262. [[CrossRef](#)]

56. Velasco LC, P.; Serquiña, R.P.; Zamad MS, A.A.; Juanico, B.F.; Lomocso, J.C. Performance analysis of multilayer perceptron neural network models in week-ahead rainfall forecasting. *Int. J. Adv. Comput. Sci. Appl.* **2019**, *10*, 578–588. [[CrossRef](#)]
57. Elias, I.; Rubio, J.D.J.; Martinez, D.I.; Vargas, T.M.; Garcia, V.; Mujica-Vargas, D.; Meda-Campaña, J.A.; Pacheco, J.; Gutierrez, G.J.; Zacarias, A. Genetic algorithm with radial basis mapping network for the electricity consumption modeling. *Appl. Sci.* **2020**, *10*, 4239. [[CrossRef](#)]
58. Ojo, O.S.; Adeyemi, B.; Oluleye, D.O. Artificial neural network models for prediction of net radiation over a tropical region. *Neural Comput. Appl.* **2021**, *33*, 6865–6877. [[CrossRef](#)]
59. Ali, Z.; Hussain, I.; Faisal, M.; Nazir, H.M.; Hussain, T.; Shad, M.Y.; Mohamd Shoukry, A.; Hussain Gani, S. Forecasting drought using multilayer perceptron artificial neural network model. *Adv. Meteorol.* **2017**, *2017*, 5681308. [[CrossRef](#)]
60. Luk, K.C.; Ball, J.E.; Sharma, A. A study of optimal model lag and spatial inputs to artificial neural network for rainfall forecasting. *J. Hydrol.* **2000**, *227*, 56–65. [[CrossRef](#)]
61. Esteves, J.T.; de Souza Rolim, G.; Ferraudo, A.S. Rainfall prediction methodology with binary multilayer perceptron neural networks. *Clim. Dyn.* **2019**, *52*, 2319–2331. [[CrossRef](#)]
62. Shah, H.; Ghazali, R. Prediction of earthquake magnitude by an improved ABC-MLP. In *2011 Developments in E-Systems Engineering*; IEEE: New York, NY, USA, 2011; pp. 312–317.
63. Yamany, W.; Tharwat, A.; Hassanin, M.F.; Gaber, T.; Hassanien, A.E.; Kim, T.H. A new multi-layer perceptrons trainer based on ant lion optimization algorithm. In Proceedings of the 2015 Fourth International Conference on Information Science and Industrial Applications (ISI), Busan, Republic of Korea, 20–22 September 2015; pp. 40–45.
64. Miksovsky, J.; Raidl, A. Testing the performance of three nonlinear methods of time series analysis for prediction and downscaling of European daily temperatures. *Nonlinear Process. Geophys.* **2005**, *12*, 979–991. [[CrossRef](#)]
65. Hernández, G.; Zamora, E.; Sossa, H.; Téllez, G.; Furlán, F. Hybrid neural networks for big data classification. *Neurocomputing* **2020**, *390*, 327–340. [[CrossRef](#)]
66. Faris, H.; Alkassabeh, M.; Rodan, A. Artificial Neural Networks for Surface Ozone Prediction: Models and Analysis. *Pol. J. Environ. Stud.* **2014**, *23*, 341–348.
67. Mukherjee, I.; Routroy, S. Comparing the performance of neural networks developed by using Levenberg–Marquardt and Quasi-Newton with the gradient descent algorithm for modelling a multiple response grinding process. *Expert Syst. Appl.* **2012**, *39*, 2397–2407. [[CrossRef](#)]
68. Fletcher, R. *Practical Methods of Optimization*; John Wiley & Sons: Singapore, 2013.
69. Asirvadam, V.S.; McLoone, S.F.; Irwin, G.W. Memory efficient BFGS neural-network learning algorithms using MLP-network: A survey. In Proceedings of the 2004 IEEE International Conference on Control Applications, Taipei, Taiwan, 2–4 September 2004; Volume 1, pp. 586–591.
70. Hery, M.A.; Ibrahim, M.; June, L.W. BFGS method: A new search direction. *Sains Malays.* **2014**, *43*, 1591–1597.
71. Sudheer, K.P.; Srinivasan, K.; Neelakantan, T.R.; Srinivas, V.V. A nonlinear data-driven model for synthetic generation of annual streamflows. *Hydrol. Process. Int. J.* **2008**, *22*, 1831–1845. [[CrossRef](#)]
72. Vivekanandan, N. Prediction of rainfall using mlp and rbf networks. *Int. J. Adv. Netw. Appl.* **2014**, *5*, 1974.
73. Chicco, D.; Warrens, M.J.; Jurman, G. The coefficient of determination R-squared is more informative than SMAPE, MAE, MAPE, MSE and RMSE in regression analysis evaluation. *PeerJ Comput. Sci.* **2021**, *7*, e623. [[CrossRef](#)]
74. Valle, M.V.; García, G.M.; Cohen, I.S.; Klaudia Oleschko, L.; Ruiz Corral, J.A.; Korvin, G. Spatial variability of the Hurst exponent for the daily scale rainfall series in the state of Zacatecas, Mexico. *J. Appl. Meteorol. Climatol.* **2013**, *52*, 2771–2780. [[CrossRef](#)]
75. Balkissoon, S.; Fox, N.; Lupo, A. Fractal characteristics of tall tower wind speeds in Missouri. *Renew. Energy* **2020**, *154*, 1346–1356. [[CrossRef](#)]
76. Taqqu, M.S.; Teverovsky, V.; Willinger, W. Estimators for long-range dependence: An empirical study. *Fractals* **1995**, *3*, 785–798. [[CrossRef](#)]
77. Kendziorowski, C.M.; Bassingthwaite, J.B.; Tonellato, P.J. Evaluating maximum likelihood estimation methods to determine the Hurst coefficient. *Phys. A Stat. Mech. Its Appl.* **1999**, *273*, 439–451. [[CrossRef](#)]
78. Feng, L.; Zhou, J. Trend predictions in water resources using rescaled range (R/S) analysis. *Environ. Earth Sci.* **2013**, *68*, 2359–2363. [[CrossRef](#)]
79. Tatli, H. Detecting persistence of meteorological drought via the Hurst exponent. *Meteorol. Appl.* **2015**, *22*, 763–769. [[CrossRef](#)]
80. Pal, S.; Dutta, S.; Nasrin, T.; Chattopadhyay, S. Hurst exponent approach through rescaled range analysis to study the time series of summer monsoon rainfall over northeast India. *Theor. Appl. Climatol.* **2020**, *142*, 581–587. [[CrossRef](#)]
81. Rao, A.R.; Bhattacharya, D. Comparison of Hurst exponent estimates in hydrometeorological time series. *J. Hydrol. Eng.* **1999**, *4*, 225–231. [[CrossRef](#)]
82. Setty, V.A.; Sharma, A.S. Characterizing detrended fluctuation analysis of multifractional Brownian motion. *Phys. A Stat. Mech. Its Appl.* **2015**, *419*, 698–706. [[CrossRef](#)]
83. Hurst, H.E. Long-term storage capacity of reservoirs. *Trans. Am. Soc. Civ. Eng.* **1951**, *116*, 770–808. [[CrossRef](#)]
84. Kanounikov, I.E.; Antonova, E.V.; Kiselev, B.V.; Belov, D.R. Dependence of one of the fractal characteristics (Hurst exponent) of the human electroencephalogram on the cortical area and type of activity. In Proceedings of the IJCNN'99. International Joint Conference on Neural Networks. Proceedings (Cat. No. 99CH36339), Washington, DC, USA, 10–16 July 1999; Volume 1, pp. 243–246.



85. Yurtseven, İ.; Serengil, Y. Changes and trends of seasonal total rainfall in the province of Istanbul, Turkey. *J. Fac. For. Istanbul Univ.* **2017**, *67*, 1–12. [[CrossRef](#)]
86. Caloiero, T.; Caloiero, P.; Frustaci, F. Long-term precipitation trend analysis in Europe and in the Mediterranean basin. *Water Environ. J.* **2018**, *32*, 433–445. [[CrossRef](#)]
87. Kastridis, A.; Kamperidou, V.; Stathis, D. Dendroclimatological Analysis of Fir (*A. borisii-regis*) in Greece in the frame of Climate Change Investigation. *Forests* **2022**, *13*, 879. [[CrossRef](#)]
88. Mersin, D.; Tayfur, G.; Vaheddoost, B.; Safari, M.J.S. Historical trends associated with annual temperature and precipitation in Aegean Turkey, where are we heading? *Sustainability* **2022**, *14*, 13380. [[CrossRef](#)]
89. Todaro, V.; D’Oria, M.; Secci, D.; Zanini, A.; Tanda, M.G. Climate change over the Mediterranean region: Local temperature and precipitation variations at five pilot sites. *Water* **2022**, *14*, 2499. [[CrossRef](#)]
90. Varlas, G.; Stefanidis, K.; Papaioannou, G.; Panagopoulos, Y.; Pytharoulis, I.; Katsafados, P.; Papadopoulos, A.; Dimitriou, E. Unravelling precipitation trends in Greece since 1950s using ERA5 climate reanalysis data. *Climate* **2022**, *10*, 12. [[CrossRef](#)]
91. Bacanlı, U.G.; Tanrikulu, A. Trends in Yearly Precipitation and Temperature on the Aegean Region, Turkey. In *Ovidius University Annals, Series Civil Engineering*; Ovidius University Press: Constanța, Romania, 2016; Volume 18.
92. Güner Bacanlı, Ü. Trend analysis of precipitation and drought in the Aegean region, Turkey. *Meteorol. Appl.* **2017**, *24*, 239–249. [[CrossRef](#)]
93. Abu Hammad, A.H.; Salameh, A.A.; Fallah, R.Q. Precipitation Variability and Probabilities of Extreme Events in the Eastern Mediterranean Region (Latakia Governorate-Syria as a Case Study). *Atmosphere* **2022**, *13*, 131. [[CrossRef](#)]
94. Balcıoğlu, Y.E.; Gönencgil, B. Trends of temperature and precipitation in the north and south of İstanbul as a transitional climate zone. In Proceedings of the TÜCAUM 2022 International Geography Symposium, Ankara, Turkey, 12–14 October 2022.
95. Drori, R.; Ziv, B.; Saaroni, H.; Etkin, A.; Sheffer, E. Recent changes in the rain regime over the Mediterranean climate region of Israel. *Clim. Chang.* **2021**, *167*, 15. [[CrossRef](#)]
96. Lionello, P.; Malanotte-Rizzoli, P.; Boscolo, R.; Alpert, P.; Artale, V.; Li, L.; Luterbacher, J.; May, W.; Trigo, R.; Tsimplis, M.; et al. The Mediterranean climate: An overview of the main characteristics and issues. *Dev. Earth Environ. Sci.* **2006**, *4*, 1–26.
97. Türkeş, M.; Deniz, Z.A. Climatology of South Marmara Division (North West Anatolia) and observed variations and trends. *J. Hum. Sci.* **2011**, *8*, 1579–1600.
98. Asikoglu, O.L.; Ciftlik, D. Recent rainfall trends in the Aegean region of Turkey. *J. Hydrometeorol.* **2015**, *16*, 1873–1885. [[CrossRef](#)]
99. Çağlıyan, A.; Gülsen, A. Spatial analysis of precipitation in Turkey. In Proceedings of the International Geography Symposium on the 30th Anniversary of TUCAUM, Ankara, Türkiye, 3–6 October 2018.
100. Atalay, I.; Efe, R. Structural and distributional evaluation of forest ecosystems in Türkiye. *J. Environ. Biol.* **2010**, *31*, 61.
101. Atalay, I. *Climate Atlas of Turkey*; İnkılap Publishing House: İstanbul, Türkiye, 2011. (In Turkish)
102. Bilgili, M.; Sahin, B. Prediction of long-term monthly temperature and rainfall in Turkey. *Energy Sources Part A* **2009**, *32*, 60–71. [[CrossRef](#)]
103. Moustris, K.P.; Larissi, I.K.; Nastos, P.T.; Paliatso, A.G. Precipitation forecast using artificial neural networks in specific regions of Greece. *Water Resour. Manag.* **2011**, *25*, 1979–1993. [[CrossRef](#)]
104. Yıldırım, A.; Yerel Kandemir, S. Prediction of Precipitation with Artificial Neural Networks. *Bilecik Şeyh Edebali Univ. J. Sci.* **2018**, *5*, 97–104.
105. Estevez, J.; Liu, X.; Bellido-Jimenez, J.A.; Garcia-Marin, A.P. Assessing Wavelet Analysis for Precipitation Forecasts Using Artificial Neural Networks in Mediterranean Coast. In Proceedings of the ITISE 2019, Granada, Spain, 25–27 September 2019; Volume 2.
106. Elbeltagi, A.; Zerouali, B.; Bailek, N.; Bouchouicha, K.; Pande, C.; Santos, C.A.G.; Towfiqul Islam, A.R.M.; Al-Ansari, N.; El-kenawy, E.S.M. Optimizing hyperparameters of deep hybrid learning for rainfall prediction: A case study of a Mediterranean basin. *Arab. J. Geosci.* **2022**, *15*, 933. [[CrossRef](#)]

**Disclaimer/Publisher’s Note:** The statements, opinions and data contained in all publications are solely those of the individual author(s) and contributor(s) and not of MDPI and/or the editor(s). MDPI and/or the editor(s) disclaim responsibility for any injury to people or property resulting from any ideas, methods, instructions or products referred to in the content.